

Dalton Transactions

Accepted Manuscript



This is an *Accepted Manuscript*, which has been through the Royal Society of Chemistry peer review process and has been accepted for publication.

Accepted Manuscripts are published online shortly after acceptance, before technical editing, formatting and proof reading. Using this free service, authors can make their results available to the community, in citable form, before we publish the edited article. We will replace this *Accepted Manuscript* with the edited and formatted *Advance Article* as soon as it is available.

You can find more information about *Accepted Manuscripts* in the [Information for Authors](#).

Please note that technical editing may introduce minor changes to the text and/or graphics, which may alter content. The journal's standard [Terms & Conditions](#) and the [Ethical guidelines](#) still apply. In no event shall the Royal Society of Chemistry be held responsible for any errors or omissions in this *Accepted Manuscript* or any consequences arising from the use of any information it contains.

Synthesis and f-element ligation properties of ^NCMPO-decorated pyridine N-oxide platforms†

Sabrina Ouizem,^a Daniel Rosario-Amorin,^a Diane A. Dickie,^a Robert T. Paine,^{a*} A. de Bettencourt-Dias,^b Benjamin P. Hay,^c Julien Podair^c and Lætitia H. Delmau^c

Stepwise syntheses for 2-{[2-(diphenylphosphoryl)acetamido]methyl}pyridine 1-oxide, 2-[Ph₂P(O)CH₂C(O)N(H)CH₂]C₅H₄NO (**6**), 2-{[2-(diphenylphosphoryl)acetamido]methyl}-6-[(diphenylphosphoryl)methyl]pyridine 1-oxide, 2-[Ph₂P(O)CH₂C(O)N(H)CH₂]-6-[Ph₂P(O)CH₂]C₅H₃NO (**7**) and 2,6-bis{[2-(diphenylphosphoryl)acetamido]methyl}pyridine 1-oxide, 2,6-[Ph₂P(O)CH₂C(O)N(H)CH₂]₂C₅H₃NO (**8**) are reported along with spectroscopic characterization data and single crystal X-ray diffraction structure determinations for **6**·2H₂O, **7** and 2,6-[Ph₂P(O)CH₂C(O)N(H)CH₂]₂C₅H₃N·MeOH **18**·MeOH, the pyridine precursor of **8**. Molecular mechanics computations indicate that **6**, **7** and **8** should experience minimal steric hindrance to donor group reorganization that would permit tridentate, tetradentate and pentadentate docking structures for the respective ligands on lanthanide cations. However, crystal structure determinations for the lanthanide complexes, {[Yb(**6**)(NO₃)₃]·(MeOH)}_n, {[Lu(**6**)(NO₃)₃]·(MeOH)}_n, [Er(**6**)₂(H₂O)₂](NO₃)₃·(H₂O)₄]_n, {[La(**13**)(NO₃)₃(MeOH)]·(MeOH)}_n, {[Eu(**7**)(NO₃)₂(EtOAc)_{0.5}(H₂O)_{0.5}](NO₃)₂·MeOH and [Dy₃(**7**)₄(NO₃)₄(H₂O)₂](NO₃)₅·(MeOH)₅·(H₂O)₂ reveal solid-state structures with mixed chelating/bridging ligand:Ln(III) interactions that employ lower than maximal denticity. The binding of **6** and **7** with Eu(III) in the solid state and in MeOH solutions is also accessed by emission spectroscopy. The acid dependence for solvent extractions by **6** and **7**, in 1,2-

dichloroethane for Eu(III) and Am(III) in nitric acid solutions is described and compared with the behavior of *n*-octyl(phenyl)-*N,N*-diisobutylcarbamoylmethylphosphine oxide (OPhDiBCMPO, **1b**) and 2-[(diphenyl)phosphinoylmethyl]pyridine *N*-oxide (DPhNOPO, **4a**)

^a*Department of Chemistry and Chemical Biology, University of New Mexico, Albuquerque, New Mexico 87131, USA*

^b*Department of Chemistry, University of Nevada, Reno, Nevada 89557, USA*

^c*Chemical Sciences Division, Oak Ridge National Laboratory, P.O. Box 2008, Oak Ridge, Tennessee 37831, United States*

**E-mail: rtpaine@unm.edu*

† Electronic supplementary information (ESI) available: Crystallographic information files (CIF) for **6**·2H₂O, **7**, **12**, **18**·MeOH and five complexes, CCDC 977749 and 977751 to 977758. NMR, IR, UV-vis and mass spectra for **6-8** and their synthetic intermediates, emission intensity decay profiles, schematic views of selected coordination complex structures and parameter files for MM3 computations (103 pages). For ESI and crystallographic data in CIF or other electronic format see DOI:

Introduction

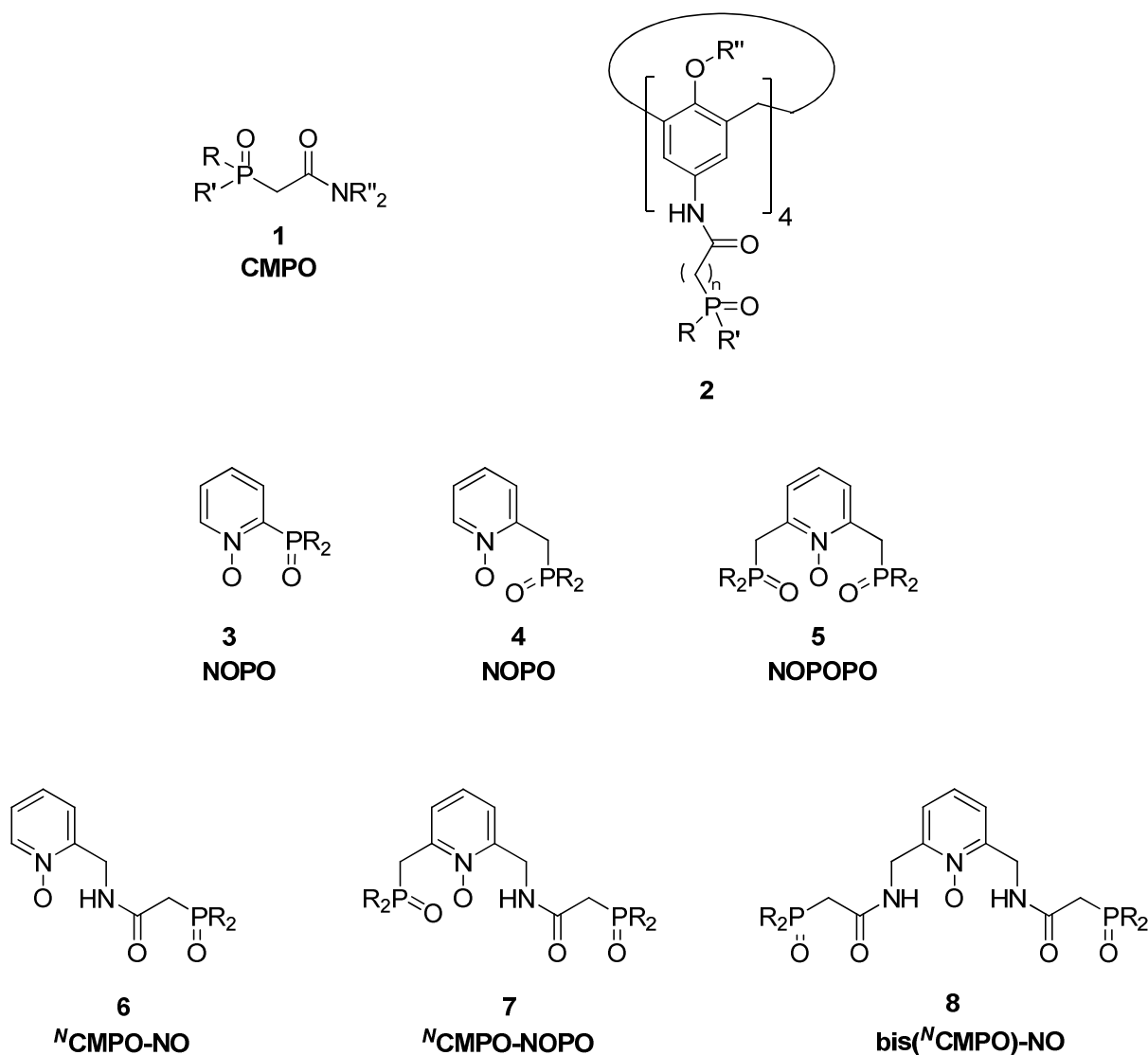
Practical needs for efficient liquid phase separations of f-block element cations have driven efforts to design and synthesize robust, donor group functionalized organic molecules that can serve as selective receptors and extractive partitioning vehicles.¹⁻⁷ Two of the more popular donor groups employed in new extractant constructs include organophosphine oxides and organoamides. Indeed, combinations of these two donor groups into hybrid bifunctional molecules have provided the well studied family of neutral carbamoylmethylphosphine oxides (CMPO), **1**, extractants. One example, (N,N-diisobutylcarbamoylmethyl)(*n*-octyl)(phenyl)phosphine oxide, OPhDiBCMPO, (R = Ph, R' = *n*-octyl, R'' = *i*-Bu) **1b**, is the key functional component in the TRUEX process^{1,2,8} for commercial separation of trivalent f-element cations from highly acidic aqueous solutions. Although the extraction performance of these bifunctional ligands has been extensively studied, the detailed solution phase compositions and structures of CMPO/f-element extraction complexes remain incompletely defined. In this regard, Boehme and Wipff⁹ have computationally evaluated the energetics of gas phase 1:1 Ln(III)-CMPO interactions, and they concluded that bidentate O_PO_C ligand binding is only slightly more stable than monodentate O_P binding. Experimentally, ligand dependency analyses for the extraction of Am(III) from nitric acid solutions suggest that the dominant extraction complex present in hydrocarbon diluents is [Am(CMPO)₃(NO₃)₃] \cdot 3HNO₃.¹⁰ Further, based upon solution NMR and IR studies of model lanthanide/CMPO complexes, it has been proposed that CMPO ligands in organic solutions coordinate in a monodentate O_P mode while the amide carbonyl O_C atom coordinates with co-extracted nitric acid.¹¹ Hence, it has been proposed that, in the presence of excess neutral CMPO molecules, charge compensating anions and solvent molecules, steric congestion in the metal ion inner coordination sphere likely results in some or

all of the CMPO ligands adopting the monodentate O_P binding mode under solvent extraction conditions. However, evidence that this binding condition may be dynamic is provided by X-ray crystal structure determinations for isolated Ln(III)-CMPO complexes. Typically, in 2:1 complexes containing nitrate counterions, the CMPO ligands bond in a bidentate $O_P O_C$ fashion on larger Ln(III) ions while with smaller Ln(III) ions they coordinate through monodentate Ln- O_P interactions.¹² In the latter cases, the amide carbonyl O-atoms hydrogen bond with an inner sphere water molecule. In one reported 3:1 complex, a crystal structure determination reveals that all three CMPO ligands bind by using monodentate Ln- O_P interactions.¹³ These findings are consistent with the proposal that the amide carbonyl center functions as an internal “buffer” facilitating phase transfer of extraction complexes.^{1,2}

The observations that multiple (probably three) CMPO ligands are present in trivalent f-element ion solvent extraction complexes have stimulated several groups to pre-organize multiple CMPO fragments on organic backbones with the goal of achieving enhanced ligand binding and extraction performance. Backbones that have been employed for this purpose include C_3 -symmetric alkyls,¹⁴⁻¹⁸ C_3 -symmetric amines,¹⁸ 1,3,5-trialkyl arenes,¹⁷ upper- and lower-rim calixarenes¹⁹ and resorcinarenes.²⁰ The organic backbone-CMPO attachment linkage, in all cases, has been made through the CMPO amide N-atom (designated as N CMPO), as schematically illustrated in the calixarene system, **2**. As expected, several of these pre-organized, multi-CMPO fragment ligands have demonstrated improved extraction performance compared to free CMPO.

Pyridine N-oxides have also been employed as simple monofunctional solvent extraction reagents,^{21,22} and we have recently used the pyridine and pyridine N-oxide rings as platforms to prepare bi- and trifunctional ligands such as represented by **3-5**.^{23,24} The extraction performance

of examples of **3** is unremarkable; they behave much like tributylphosphine oxide.²⁵ On the other hand, examples of **4** and especially **5** show markedly improved extraction performance compared to pyridine N-oxide, CMPs and CMPOs.²⁶ The successes realized with examples of **4** and **5** led us to consider options for linking CMPO fragments on pyridine N-oxide platforms such that the hybrid ligands might form multidentate chelate interactions with Ln(III) and An(III) ions resulting in improved solvent extraction behavior. There are several synthetic options for linking the CMPO and pyridine N-oxide fragments including through the CMPO P-atom, the CMPO

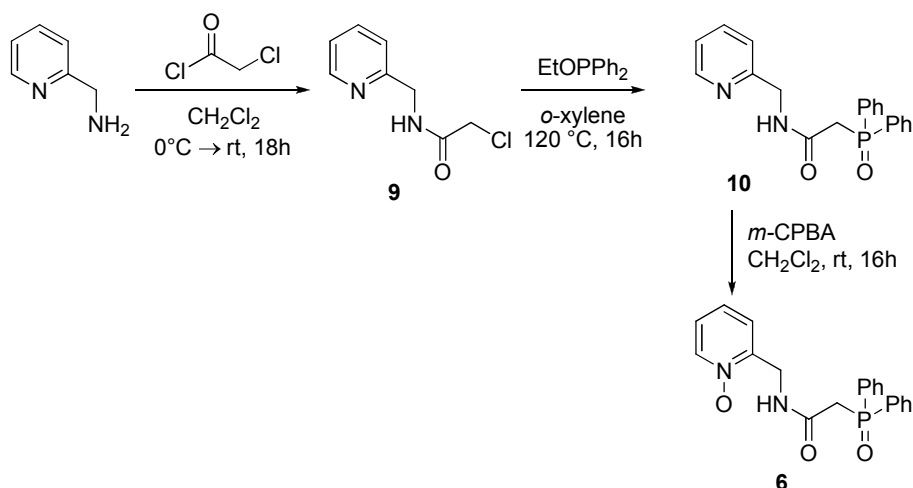


methylene C-atom and the CMPO N-atom. We have recently described initial progress on the study of selected C-attached (^CCMPO) options,²⁷ and in the current contribution we outline syntheses for three new classes of ligands, **6**, **7** and **8** (R = phenyl), that employ N-attached (^NCMPO) linkages via the CMPO amide N-atom site and the 2-methylpyridine N-oxide platform. In addition, selected lanthanide coordination chemistry of the new ligands, and preliminary Eu(III) and Am(III) solvent extraction analyses for **6** and **7** are described.

Results and discussion

Ligand syntheses and characterization

The first hybrid ^NCMPO-NO ligand targeted for synthesis was compound **6**. It was selected in order to determine the impact on the CMPO binding by placement of a 2-methylpyridine N-oxide fragment on the amide functionality. The compound was obtained in 53 % overall yield via a three-step sequence summarized in Scheme 1. This procedure is similar to that used previously for the synthesis of C₃-symmetric ^NCMPO-decorated arenes.¹⁷ Syntheses for the intermediate, **9** and its hydrochloride salt, have been previously reported.^{28,29} However, modifications used in the present study provide **9** with a slightly higher yield (94 %), and the spectroscopic data are in good agreement with data in the literature.^{28,29} The phosphine oxide, **10**, was obtained as a solid, in good yield (86 %), from an Arbusov reaction of **9** by using Ph₂POEt in refluxing *o*-xylene. The new compound displays a single ³¹P resonance, δ_P 30.5, comparable to the shift reported for the CMPO compound, **1** (R = R' = Ph, R'' = Et), δ_P 27.9.³⁰ The ¹H and ¹³C NMR parameters for the methylene groups, P(O)-CH₂-C(O) and Pyr-CH₂-N(H), reflect their electronic environments, appearing at δ_H 3.42 (J_{HP} = 12.9 Hz), δ_C 38.9 (J_{CP} = 60.4 Hz) and δ_H



Scheme 1. Synthesis of **6**.

4.44 ($J_{\text{HH}} = 5.7$ Hz), δ_{C} 45.1, respectively. The infrared spectrum for **10** contains strong absorptions at 1668 and 1177 cm^{-1} that are assigned to ν_{CO} and ν_{PO} , respectively, and these frequencies can be compared with data obtained for **1a** ($\text{R} = \text{R}' = \text{Ph}$, $\text{R}'' = \text{Et}$): ν_{CO} 1630 cm^{-1} and ν_{PO} 1205 cm^{-1} .³⁰ The N-oxidation of the pyridine fragment with *m*CPBA was efficient, and **6** was isolated as a white solid (65 %). The composition of the solid, as indicated by CHN elemental analyses, agrees relatively well with that for a monohydrate, $\mathbf{6}\cdot\text{H}_2\text{O}$. The relevant NMR parameters for **6**, δ_{P} 29.8, δ_{H} 3.47 ($J_{\text{HP}} = 13.5$ Hz), 4.51 ($J_{\text{HH}} = 6.0$ Hz) and δ_{C} 39.1 ($J_{\text{CP}} = 59.1$ Hz), 39.3, are little modified compared to the NMR data for **10**, and similar small variations have been previously observed when comparing NMR data for other NPO and NOPO-type compound pairs.²⁴ The IR spectrum for **6** also shows only small shifts for ν_{CO} and ν_{PO} following N-oxidation, and an additional, weak absorption at 1245 cm^{-1} is tentatively ascribed to ν_{NO} . Confirmation of the structure of **6** is provided by a single crystal X-ray diffraction structure determination. A view of the molecule is shown in Figure 1, and selected bond lengths are provided in Table 1. The structure determination reveals that the single crystals are obtained as a

dihydrate, $6 \cdot 2\text{H}_2\text{O}$, instead of the monohydrate indicated by CHN analysis. This suggests that one of the lattice water molecules is less tightly bound and is lost during sample handling. Each of the ligand donor O-atoms participates in hydrogen bonding to different water molecules in the unit cell (non-bonded donor/acceptor distance range: $\text{O} \cdots \text{O}$ 2.719(2)-2.762(2) Å; angle range 163-172°) with the shortest interaction, as expected, involving the stronger Lewis base site, the phosphine oxide O-atom. The pyridine N-oxide ring is planar, and the appended CMPO arm is twisted in a manner such that the three donor dipoles are pointed away from each other most likely in response to intramolecular dipole-dipole repulsions. The respective donor group bond lengths, P1-O3 1.485(1) Å, C7-O2 1.228(2) Å and N1-O1 1.325(2) Å, are typical of bond lengths in related CMPO- and NOPO-class molecules.^{24, 31}

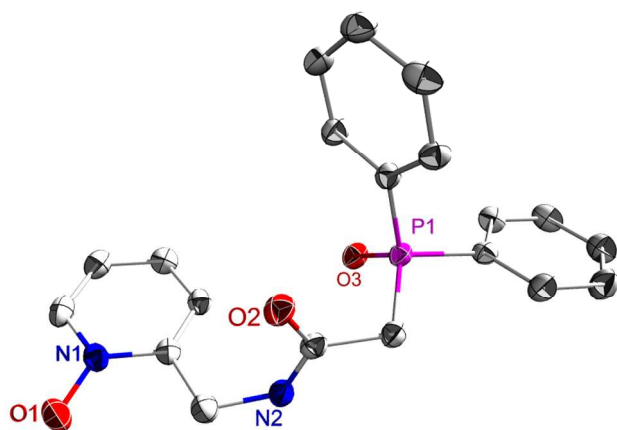
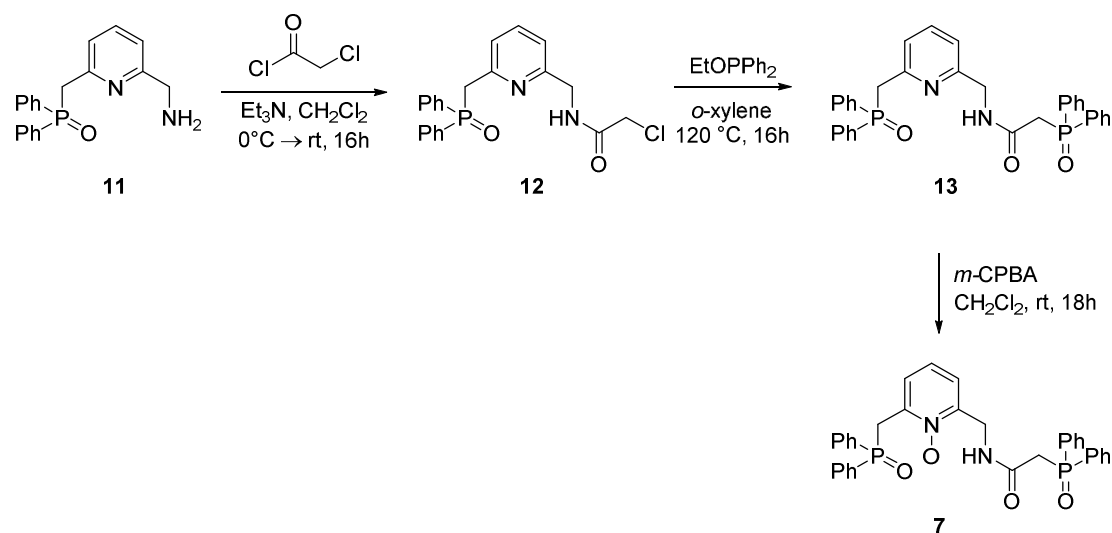


Figure 1. X-ray crystal structure of $6 \cdot 2\text{H}_2\text{O}$ (thermal ellipsoids, 50%) with H atoms and hydrogen-bonded lattice water molecules omitted for clarity. Color scheme: blue = N, red = O, lilac = P, gray = C.

[Insert Table 1 somewhere near here]

The second target hybrid ligand of interest was the ^NCMPO-NOPO compound, **7**. It can be considered to be a further modification on the structure of **6** or a modified variant of the NOPO structure, **4**. The compound was obtained as a yellow solid in 46 % overall yield via the reaction sequence outlined in Scheme 2. The spectroscopic data for the intermediates **12** and **13**, as well as **7**, are comparable with data for **9**, **10** and **6**, respectively, and a spectroscopic summary is provided in Electronic supplementary information (ESI) (Table S. 69). It is important to note that two ν_{PO} modes are observed in the FTIR spectrum for **7**: 1198 and 1173 cm^{-1} , although only one broad band is resolved for **13** at 1178 cm^{-1} . Similar to **6**, a weak absorption for **7** was observed at 1246 cm^{-1} that is tentatively ascribed to ν_{NO} . There are two resolved, equal intensity resonances in the ³¹P NMR spectrum for **7**, δ_{P} 31.4, 29.4, and for its precursor, **13**, δ_{P} 30.7, 29.7. The more upfield resonance in each molecule is assigned to the P-atom in the CMPO fragment. This assignment is consistent with the ³¹P chemical shifts displayed by the separate molecular fragments: **1a** (R = Ph) δ_{P} 27.9; **4** (R = Ph) δ_{P} 31.7. The molecular structure



Scheme 2. Synthesis of **7**

of **7** was further confirmed by single crystal X-ray diffraction analysis. A view of the molecule is shown in Figure 2, and selected bond lengths are listed in Table 1. The pyridine N-oxide ring is planar, and the appended arms are twisted in response to intramolecular repulsions between the donor groups. In addition, the molecular units display weak intermolecular hydrogen bonding interactions between the amide H-atoms and the phosphine oxide O-atoms in neighboring molecules: (donor/acceptor distance 2.926(2) Å; angle 168.2°). The respective donor group bond lengths, P1-O3 1.485(1), P2-O4 1.495(1), C7-O2 1.227(2) and N1-O1 1.308(2) Å, are similar to those observed for **6**.

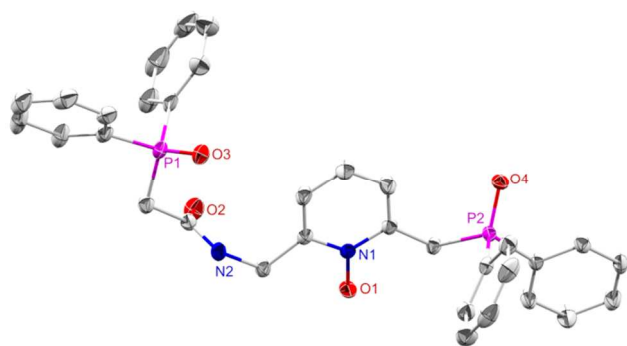


Figure 2. X-ray crystal structure of **7** (thermal ellipsoids, 50%) with H-atoms and H-bonding interactions omitted for clarity. Color scheme: blue = N, red = O, lilac = P, gray = C.

Since compound **12** is a potentially useful building block in other ligand assemblies, its molecular structure was also confirmed by single crystal X-ray diffraction analysis. A view of the molecule is shown in Figure 3, and selected bond lengths are listed in Table 1. As expected, both of the P=O and C=O bond vectors are twisted out of the pyridine ring plane, and there is a relatively strong intermolecular hydrogen bonding interaction in the unit cell between the amide N(H) group in one molecule and the carbonyl O-atom in a second molecule.

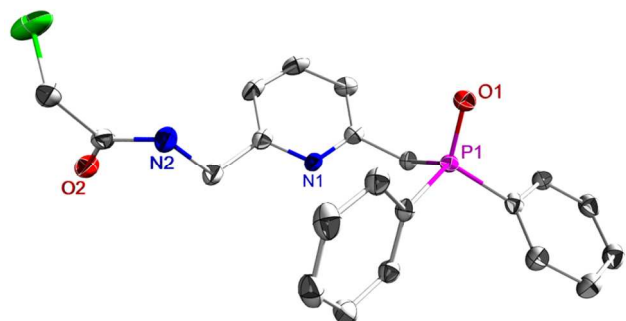
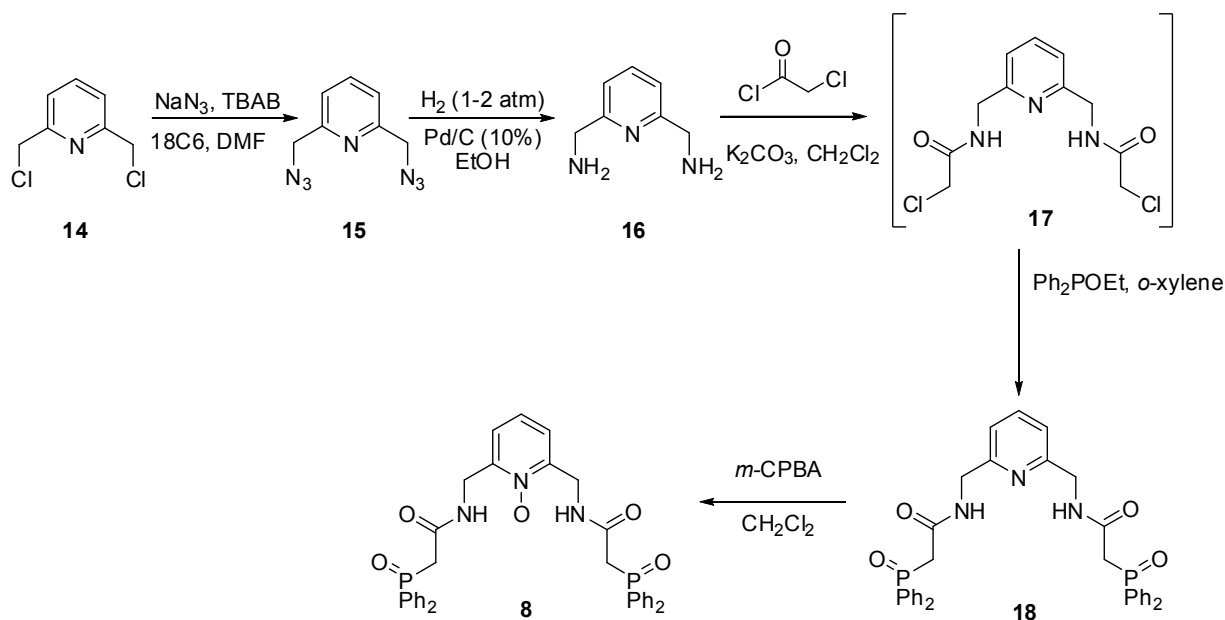


Figure 3. X-ray crystal structure of **12** (thermal ellipsoids, 50%) with H-atoms and H-bonding interactions omitted for clarity. Color scheme: blue = N, red = O, lilac = P, green = Cl, gray = C.

The bis-(^NCMPO)-NO ligand **8**, with two tethered ^NCMPO fragments on the pyridine N-oxide platform, was also selected for study, and it was obtained as a white solid in four steps from 2,6-bis(chloromethyl)pyridine, with an overall yield of 53 %, as depicted in Scheme 3. Descriptions of syntheses for intermediates **14**³² and **15**³³ have appeared in the literature. In an alternative approach, the intermediate bis-acylation compound, **17**, was isolated, and an Arbusov reaction on the isolated acyl chloride gave **18**. However, this method produces more side-products than the direct, one-pot conversion of **16** to **18**. Compound **18** is reasonably soluble in polar solvents, and CHN analyses agree with a composition corresponding to a trihydrate. Compound **8**, on the other hand, displays low solubility, it is difficult to purify and it was not obtained in analytically pure form. Nonetheless, the compositions of both **18** and **8** are supported by HRMS and NMR spectra. Single crystal X-ray analysis for **18**·MeOH was completed, and a view of the molecule is shown in Figure 4. Selected bond lengths are provided in Table 1. It is interesting that the CMPO donor



Scheme 3. Synthesis of **8**

groups are positioned on the same side of the pyridine ring plane, and it appears that they may require only minimal reorganization energy to adopt a tetradentate $(\text{O}_2\text{COP})_2$ binding configuration. This, in turn, suggests that perhaps a pentadentate chelate interaction may be accessible with **8**.

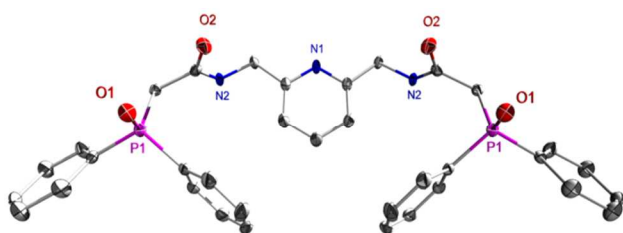


Figure 4. X-ray crystal structure of **18**·MeOH (thermal ellipsoids, 50%) with H-atoms, the lattice MeOH molecule and H-bonding interactions omitted for clarity. Color scheme: blue = N, red = O, lilac = P, gray = C.

Computational modeling

Given the results from the crystal structure determinations for **6** and **7**, it appears that, at least in the solid state, these receptor ligands may be less than optimally preorganized to adopt maximal tridentate (**6**) or tetradentate (**7**) chelate interactions on a Ln(III) cation. Therefore, the energetics of structural reorganization required for chelate formation by these compounds were computationally explored by using a force field-based structure scoring approach described previously.³⁴ The conformer search process for **6** and **7** led to the computed, energy minimized gas phase structures shown in Figures 5(a) and 6(a), respectively. As expected, the donor groups in the computed structures are rotated away from each other largely in response to intramolecular dipole-dipole repulsions. Corresponding ball and stick representations for the observed solid state structures are shown in Figures 5(b) and 6(b). It is immediately apparent that the solid state structures do not exactly overlay the computed, energy minimized gas phase structures, and the energies required to stabilize the solid state structures are provided by the intermolecular hydrogen bonding interactions discussed above and crystal packing forces. In the case of **6**, the computed solid state form is 6.5 kcal/mol higher in energy than the low-energy, gas phase form. In **7**, the related reorganization energy is 7.2 kcal/mol. A medium-sized lanthanide(III), Eu(III), cation was then offered to each ligand, initially in its low energy, gas phase conformation, and structures sought for 1:1 complexes with low conformational energy, low degrees of induced strain and minimal restricted bond rotations. The resulting lowest energy tridentate binding motif discovered for **6** is depicted in Figure 5(c) for which the calculated relative strain free energy (G) is 2.14 kcal/mole/donor group. For **7**, the lowest energy tetradentate binding state is shown in Figure 6(c), and the computed relative strain free energy is $G = 1.98$ kcal/mole/bond. These

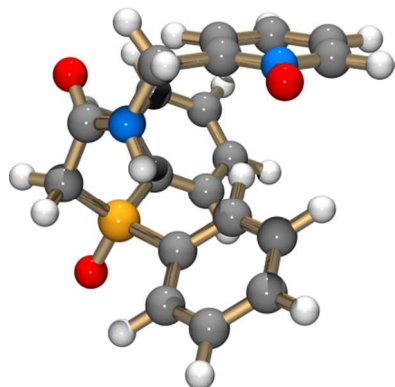
results suggest that ligand steric strain should *not* preclude $O_C O_P O_N$ tridentate chelation by **6** or $O_C O_P O_N O_P$ tetradentate chelation by **7**, at least on medium-sized Ln(III) ions.

The gas phase 1:1 interactions of **18** and **8** with Eu(III) were also computationally assessed in order to evaluate the strain encountered in adopting potential pentadentate $(O_P O_C)_2 N$ and $(O_P O_C)_2 O_N$ chelate structures, respectively. It is found that **18** can't adopt a pentadentate $(O_P O_C)_2 N$ chelate condition with use of a set of reasonable Eu-donor atom bond lengths. Only a tetradentate, $(O_P O_C)_2$, chelate structure provides reasonable connectivity. Views of the computed lowest energy structure forms for tetradentate **18**³⁵ and pentadentate **8** chelates are provided in the ESI (S. 89). The computed relative strain free energies for these structures are 4.35 and 4.20 kcal/mole/donor, respectively. Therefore, both compounds would be expected to encounter greater, but manageable, steric reorganization constraints in adopting these high denticity structures compared to the energetics predicted for **6** and **7**.

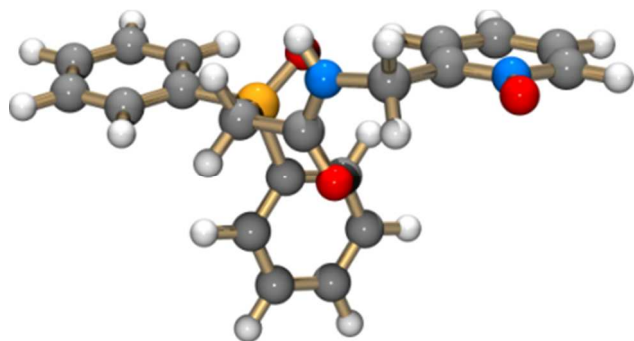
Lanthanide ion ligation

The results from the ligand steric modeling analyses are consistent with expectations that these hybrid ligands should be capable of forming stable, high denticity ligand-lanthanide interactions although maximal pentadentate chelation would not be expected to result with **18**. With this in mind, the coordination chemistry of the pyridine-based ligand, **13**, and the pyridine N-oxide-based ligands, **6**, **7**, and **8** was surveyed with early and late Ln(III) ions. Equimolar combinations of **13**, **6**, and **7** with $[Ln(NO_3)_3] \cdot nH_2O$ (Ln = La, Pr, Eu, Yb) in MeOH readily produce solid, powders with the general composition $[Ln(L)(NO_3)_3]$. The complexes, as isolated, contain varying amounts of labile lattice solvent molecules, water or methanol. The lability of the lattice

(a)



(b)



(c)

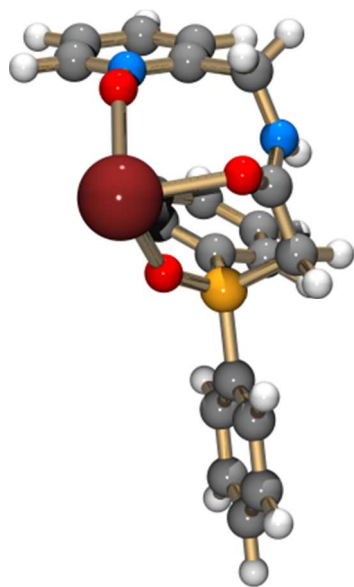
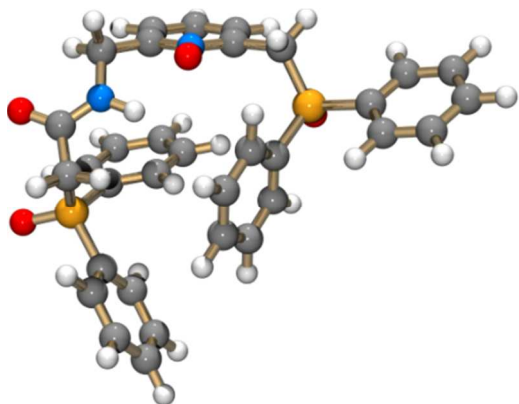


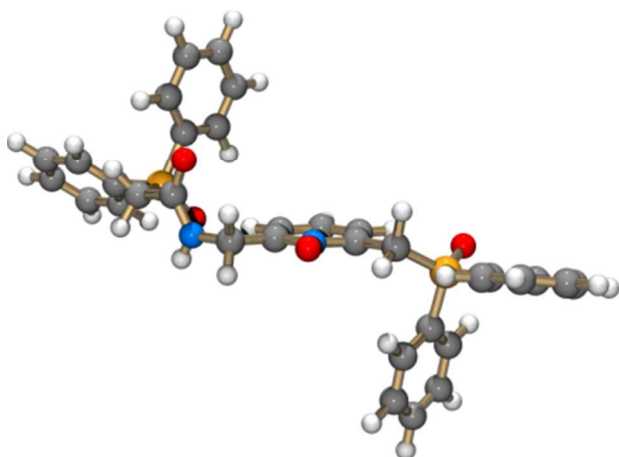
Figure 5. (a) Computed lowest energy form, (b) X-ray crystal structure form and (c) lowest energy form of tridentate coordinated **6** on Eu(III). MM3 ligand strain energies for the X-ray

conformation (b) and the bound form (c) relative to the global minimum (a) are 6.5 and 5.2 kcal/mol, respectively.

(a)



(b)



(c)

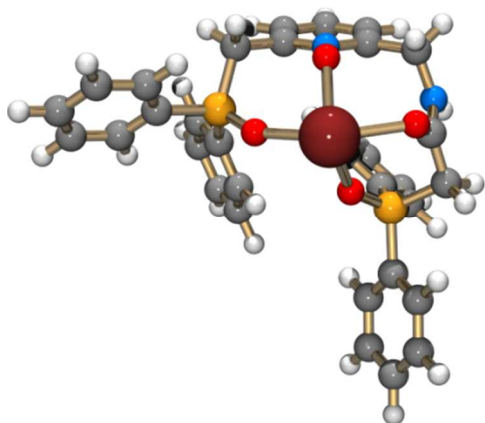


Figure 6. (a) Computed lowest energy form, (b) X-ray crystal structure form and (c) lowest energy form of tetradentate coordinated **7** on Eu(III). MM3 ligand strain energies for the X-ray conformation (b) and the bound form (c) relative to the global minimum (a) are 7.2 and 6.0 kcal/mol, respectively.

solvent molecules produce variable CHN analyses, but the results are in general agreement with the 1:1 ligand:metal composition. Infrared spectra for the complexes obtained with the pyridine-based ligand **13** show coordination shifts in the ranges $\Delta\nu_{\text{P=O}} = 21\text{-}24\text{ cm}^{-1}$ and $\Delta\nu_{\text{C=O}} = 38\text{-}42\text{ cm}^{-1}$ consistent with binding by both P=O and C=O donor groups to Ln(III) ions although the ligand denticity remains undetermined. Complexes formed with the ligands based upon the pyridine N-oxide platform, **6** and **7**, display coordination shifts $\Delta\nu_{\text{P=O}} = 14\text{-}19\text{ cm}^{-1}$, $\Delta\nu_{\text{C=O}} = 32\text{-}35\text{ cm}^{-1}$, $\Delta\nu_{\text{N=O}} = 15\text{-}17\text{ cm}^{-1}$ and $\Delta\nu_{\text{P=O}} = 13\text{-}14\text{ cm}^{-1}$, $\Delta\nu_{\text{C=O}} = 31\text{-}41\text{ cm}^{-1}$, $\Delta\nu_{\text{N=O}} = 29\text{-}33\text{ cm}^{-1}$, respectively. It is noted that the coordination shifts that indicate phosphine oxide binding are smaller than the carbonyl group coordination shifts and smaller than typically observed with several Ln/NOPO and Ln/NOPOPO complexes, $\Delta\nu_{\text{P=O}} = 50\text{-}70\text{ cm}^{-1}$.²⁴ This suggests weakened Ln-O=P interactions. A similar unexpected observation was made with Ln(III) complexes formed by a one-armed ^CCMPO- pyridine N-oxide ligand reported recently.²⁷ In contrast, typical coordination shifts for bidentate Ln(III)/CMPO, **1a** (R = R' = Ph), complexes are $\Delta\nu_{\text{P=O}} = \sim 55\text{ cm}^{-1}$ and $\Delta\nu_{\text{C=O}} = \sim 40\text{ cm}^{-1}$.³⁰

Equimolar combinations of **8** with $[\text{Ln}(\text{NO}_3)_3] \cdot n\text{H}_2\text{O}$ (Ln = La, Pr, Eu, Yb) in MeOH solution also produce solid powder complexes with varying amounts of MeOH and/or water as lattice solvents. Infrared spectra for these complexes display coordination shifts of $\Delta\nu_{\text{P=O}} = 47\text{-}61\text{ cm}^{-1}$, $\Delta\nu_{\text{C=O}} = 41\text{-}43\text{ cm}^{-1}$ and $\Delta\nu_{\text{N=O}} = 2\text{-}14\text{ cm}^{-1}$. These shifts suggest that the ligands are coordinating with similar strengths through the carbonyl and phosphoryl donor groups. On the other hand, the small $\Delta\nu_{\text{N=O}}$ shifts suggest that the pyridine N-oxide donor in **8** probably is not involved in

coordination interactions although, as indicated in earlier studies of NOPO and NOPOPO complexes,²⁴ the N-oxide stretching frequency is particularly difficult to confidently assign due to its relatively low intensity and potential overlap with nitrate ion vibrations.

Photophysical characterization

Additional information about the inner sphere coordination structure for two of the complexes was gained from emission spectroscopy. Spectroscopic data for $[\text{Eu}(\mathbf{6})(\text{NO}_3)_3]$ and $[\text{Eu}(\mathbf{7})(\text{NO}_3)_3]$ show that both complexes emit europium-centered red light in the solid state and in methanol solution upon excitation around 275-284 nm, which corresponds to sensitized emission through the coordinated ligand. The excitation spectrum for $[\text{Eu}(\mathbf{6})(\text{NO}_3)_3]$ (not shown) displays, in addition to the broad excitation bands in the range 275-350 nm, narrow $f-f$ excitation lines indicating that, for this complex, direct Eu(III) excitation is also moderately efficient. The excitation spectrum for $[\text{Eu}(\mathbf{7})(\text{NO}_3)_3]$ (not shown) only displays ligand-based excitation bands in the range 265-325 nm. The emission spectra for $[\text{Eu}(\mathbf{6})(\text{NO}_3)_3]$ are shown in Figure 7. Both

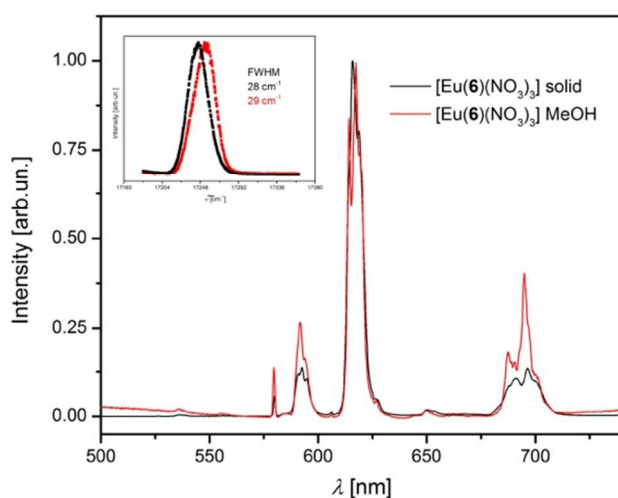


Figure 7. Emission spectra for crystalline (black trace) and methanol solution (red trace) samples of $[\text{Eu}(\mathbf{6})(\text{NO}_3)_3]$ at 77 K; $\lambda_{\text{exc}} = 284 \text{ nm}$; $[\text{complex}] \sim 1.5 \times 10^{-3} \text{ M}$.

solution and solid-state spectra display ${}^5D_0 \rightarrow {}^7F_J$ ($J = 0, 1, 2, 3, 4$) transitions, including the forbidden ${}^5D_0 \rightarrow {}^7F_0$ transition, indicating low symmetry surroundings for the europium ion and absence of an inversion center in both conditions.³⁶ The splitting of each individual peak as well as the relative intensities of the magnetic-dipole allowed ${}^5D_0 \rightarrow {}^7F_1$ and hypersensitive ${}^5D_0 \rightarrow {}^7F_2$ transitions are different in the solid state and in solution, consistent with slightly different coordination environments for the europium; in the solid state, the ligand and very likely the nitrate counter-anions are present in the first coordination sphere, while in methanol solution solvent molecules are expected to replace the nitrate counter-anions.

The analogous emission spectra for $[\text{Eu}(\mathbf{7})(\text{NO}_3)_3]$ are displayed in Figure 8. They show sensitized europium-centered emission corresponding to the ${}^5D_0 \rightarrow {}^7F_J$ ($J = 0, 1, 2, 3, 4$) transitions, including the forbidden ${}^5D_0 \rightarrow {}^7F_0$ transition consistent with a low symmetry environment around the metal ion and absence of an inversion center, both in solution and in the solid state. This is further evidenced by how the crystal field differently affects the peak splitting and the relative intensities of the magnetic-dipole allowed ${}^5D_0 \rightarrow {}^7F_1$ and hypersensitive ${}^5D_0 \rightarrow {}^7F_2$

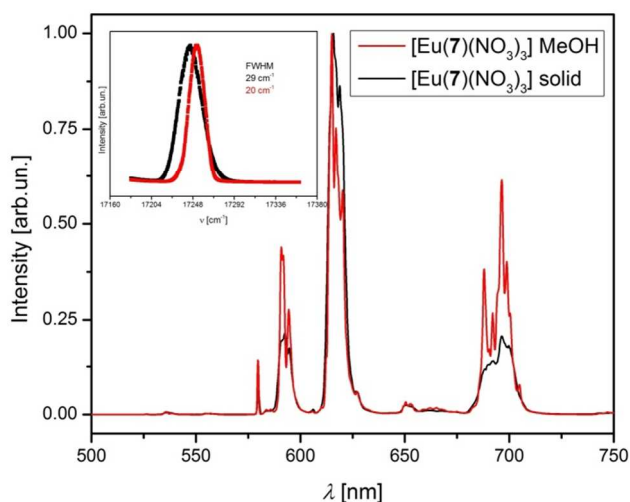


Figure 8. Emission spectra for crystalline (black trace) and methanol solution (red trace) samples of $[\text{Eu}(\mathbf{7})(\text{NO}_3)_3]$; $\lambda_{\text{exc}} = 275 \text{ nm}$, 77 K ; $[\text{complex}] \sim 1.5 \times 10^{-3} \text{ M}$.

transitions in solution and solid state, indicative of slightly different coordination environments for the europium. Descending symmetry considerations³⁷ and the splitting of the ${}^5\text{D}_0 \rightarrow {}^7\text{F}_1$ transition into up to three components and of the ${}^5\text{D}_0 \rightarrow {}^7\text{F}_2$ transition into up to five components indicate that the europium ion is, in all four systems, in a low symmetry environment, possibly C_1 , C_s , C_2 or C_{2v} . A similar behavior was seen for related Eu(III) complexes with a hybrid carbon-attached ${}^C\text{CMPO/NOPOPO}$ ligand.²⁷ The low symmetry environment around the Eu(III) ion translates into the appearance of the ${}^5\text{D}_0 \rightarrow {}^7\text{F}_0$ transition band in the emission spectrum, as well as crystal field splitting of the other bands. However, in the solid state, the band for the ${}^5\text{D}_0 \rightarrow {}^7\text{F}_0$ transition is absent and little crystal field splitting is observed. This suggests a more symmetric environment around the metal ion in the presence of **7** compared to **6**. The ${}^5\text{D}_0 \rightarrow {}^7\text{F}_0$ transition is moderately narrow for all four systems, with the full-width-at-half-maximum (*fwhm*) of 20 and 28/29 cm^{-1} , as is shown in the insets of Figures 7 and 8, and these are consistent with only one coordination environment for the Eu(III) ions.³⁸ The slight broadening observed in these spectra, as compared to reported *fwhm* in the range 15-20 cm^{-1} at similar low temperatures,³⁹ is most likely due to small vibrational distortions of the coordination environment around the Eu(III) ion, as the lifetime measurements (*vide infra*) are consistent with the presence of one species only.

The lifetimes of the complexes in the solid state as well as in methanol solution at 25°C are summarized in Table 2. The emission intensity decays as a function of time can all be fit to single exponentials, (see ESI, Figure S.88), and they indicate lifetimes of 562 and 875 μs for the complexes of Eu(III) with ligands **6** and **7** in the solid state, respectively. In methanol solution, as

nitrate ions are replaced by methanol molecules that are capable of quenching the emissive Eu(III) level through the OH vibration,⁴⁰ the lifetimes decrease to 380 and 782 μs , respectively. When methanol is replaced by deuterio-methanol, lifetimes are increased to 1.3 and 1.7 ms, respectively, since the OD vibrations are less likely to quench the $^5\text{D}_0$ state. Input of these lifetimes into Horrocks' equation⁴¹ shows that, for the complex with the potentially tridentate ligand **6**, four methanol molecules replace the three nitrate ions in the first coordination sphere of the Eu(III) in solution. This is analogous to observations made for Eu(III) complexes with the hybrid carbon-attached tridentate $^{\text{C}}$ CMPO/NOPOPO ligand.²⁷ On the other hand, ligand **7**, only shows coordination of approximately 1.5 methanol molecules in the first coordination sphere of Eu(III). This agrees well with a more shielded coordination environment provided by the bulkier tetradentate ligand structure calculated for this complex and shown in Figure 6c.

[Insert Table 2 near here]

Crystal Structure Analyses.

Although useful for indicating likely donor group coordination interactions, the IR and emission spectroscopic data alone do not permit unambiguous assignments of ligand denticities in solution or the solid state for coordination complexes that contain ligands with structurally complex donor atom fields. Therefore, attempts were also made to grow single crystals and complete X-ray diffraction analyses for representative solid state complexes. Suitable crystals for $\{[\text{Yb}(\mathbf{6})(\text{NO}_3)_3]\cdot(\text{MeOH})\}_n$ were isolated, and a view of the linear chain structure containing nine coordinate Yb(III) ions is shown in Figure 9.⁴² Selected bond lengths are provided in Table 3. The key structural observation is that the relatively small Yb(III) ion (effective ionic radius = 0.98 Å, CN = 8)⁴³, bonds in the inner coordination sphere with three asymmetric bidentate nitrate

anions and one neutral ligand **6** that adopts a relatively symmetric *bidentate* O_PO_C interaction by using the appended CMPO fragment: Yb-O_P 2.271(3) Å, Yb-O_C 2.268(3) Å. The [Yb(**6**)(NO₃)₃] units are linked via *bridge* bonds, Yb-O_N, 2.241(3) Å, formed by the pyridine N-oxide O-atom from another [Yb(**6**)(NO₃)₃] unit.

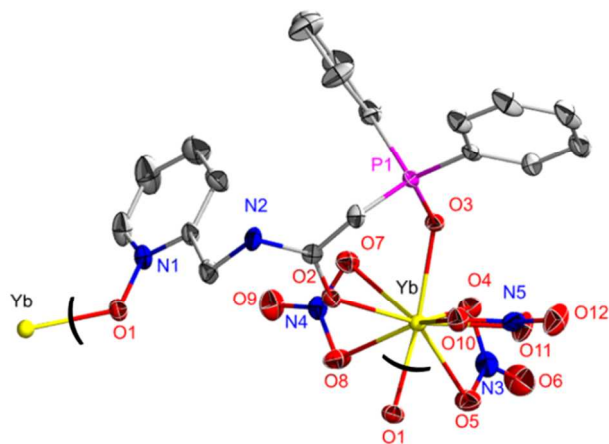


Figure 9. X-ray crystal structure of {[Yb(**6**)(NO₃)₃](MeOH)}_n (thermal ellipsoids, 50%) with C-atom labels, H-atoms and lattice MeOH omitted for clarity. Color scheme: blue = N, red = O, lilac = P, gray = C, yellow = Yb.

[Insert Table 3 somewhere near here]

The 1:1 combination of **6** with Er(NO₃)₃·nH₂O in MeOH solution results in formation of a complex from which single crystals are obtained by slow evaporation of the solution. Unexpectedly, the X-ray diffraction analysis reveals formation of a complex with a 2:1 composition, {[Er(**6**)₂(H₂O)₂](NO₃)₃·(H₂O)₄}_n. A view of the inner coordination sphere of the 1-D polymeric structure is provided in Figure 10,⁴² and selected bond lengths are listed in Table 3. Each Er(III) ion is eight coordinate with the inner sphere positions occupied by O-atoms from two equivalent, asymmetrically bonded bidentate CMPO fragments, Er-O_P, 2.272(3) Å and Er-

O_C 2.430(3) Å, two bridging pyridine N-oxide O-atoms from neighboring $[Er(\mathbf{6})_2(H_2O)_2]$ fragments, $Er-O_N$, 2.324(3) Å, and two water molecules, $Er-O_w$ 2.365(3) Å. The three nitrate

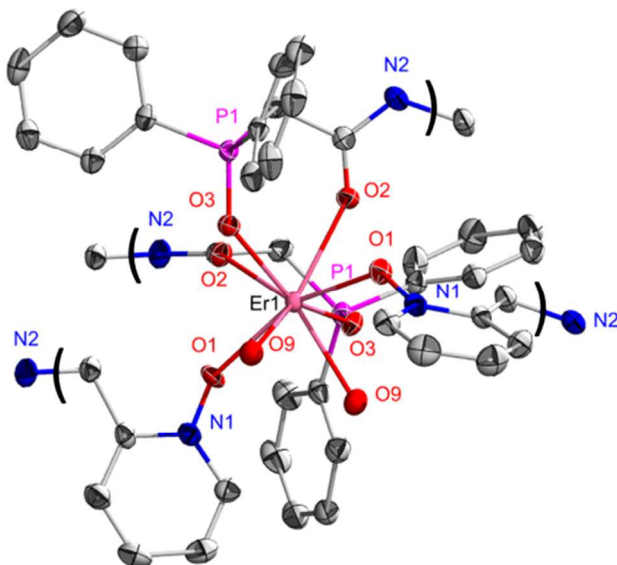


Figure 10. X-ray crystal structure of $\{[Er(\mathbf{6})_2(H_2O)_2](NO_3)_3 \cdot (H_2O)_4\}_n$ (thermal ellipsoids, 50%) with H-atoms and lattice MeOH omitted for clarity. Color scheme: blue = N, red = O, lilac = P, gray = C, pink = Er.

counter-ions for each Er(III) are rejected into the outer sphere. These observations suggest that, in solid state complexes, despite a relatively low strain energy per donor group, **6** prefers to adopt an $O_P O_C$ bidentate + bridge O_N binding mode over the tridentate $O_P O_C O_N$ interaction with late Ln(III) ions. This does not rule out that a tridentate chelate interaction may appear in complexes of **6** with earlier, larger Ln(III) ions in solution or the solid state. However, at this time, diffraction quality crystals of an early lanthanide complex, Ln = La, Pr or Eu, containing **6** have not yet been obtained.

The structure analysis for crystals grown from the initially formed 1:1 complex $[Eu(\mathbf{7})(NO_3)_3]$ reveals a composition, $\{[Eu(\mathbf{7})(NO_3)_2(EtOAc)_{0.5}(H_2O)_{0.5}] (NO_3)_2 \cdot (MeOH)\}$. The structure is

dimeric as illustrated in the ORTEP view shown in Figure 11,⁴² and selected bond lengths are given in Table 3. Each Eu(III) ion is nine coordinate with the coordination positions occupied by

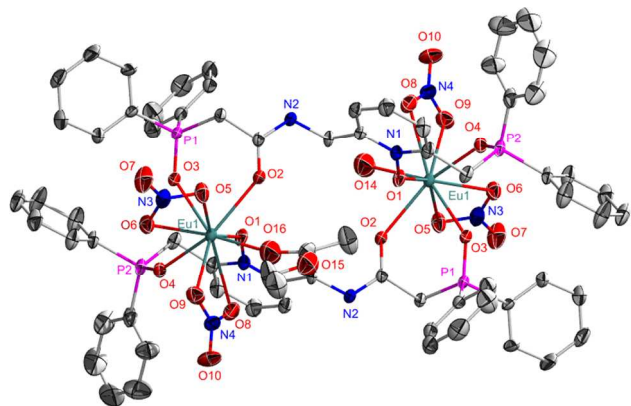


Figure 11. X-ray crystal structure and atom labeling scheme for $\{[\text{Eu}(\mathbf{7})(\text{NO}_3)_2(\text{EtOAc})_{0.5}(\text{H}_2\text{O})_{0.5}](\text{NO}_3)\}_2 \cdot (\text{MeOH})$ (thermal ellipsoids, 50%) with carbon atom labels, H-atoms and lattice nitrate ions and methanol omitted for clarity. Color scheme: blue = N, red = O, lilac = P, gray = C, turquoise = Eu.

two O-atoms from a bidentate NOPO fragment of one molecule of **7**, Eu1-O4_P 2.350(2) Å and Eu1-O1_N 2.322(2) Å, two O-atoms provided by a bidentate CMPO fragment in a second molecule of **7**, Eu1-O3_P 2.381(2) Å and Eu1-O2_C 2.444(3) Å, four O-atoms from two asymmetric, bidentate nitrate ions and an O atom from a disordered solvent molecule (half occupancy each of a EtOAc, Eu1-O16 2.349(8) Å and a water molecule, Eu1-O14 2.497(7) Å). The remaining two nitrates and a MeOH molecule reside in the outer sphere.

Crystallization of a 1:1 complex formed by $\text{Dy}(\text{NO}_3)_3 \cdot n\text{H}_2\text{O}$ and **7** from methanol gave single crystal for which X-ray structure analysis provides a composition $[\text{Dy}_3(\mathbf{7})_4(\text{NO}_3)_4(\text{H}_2\text{O})_2](\text{NO}_3)_5 \cdot (\text{MeOH})_5 \cdot (\text{H}_2\text{O})_2$. An ORTEP view of the monomer unit of the linear chain structure is displayed in Figure 12,⁴² and selected bond lengths are given in Table 3. The central Dy(III) ion, Dy2, is eight coordinate with the coordination sphere generated by

bidentate NOPO fragments from two molecules of **7**, Dy2-O8_P 2.378(7) Å, Dy2-O5_N 2.346(7) Å and by two bidentate CMPO fragments from two different molecules of **7**, Dy2-O3_P 2.311(7) Å and Dy2-O2_C 2.446(7) Å. The outer two Dy(III) ions are equivalent and each is nine

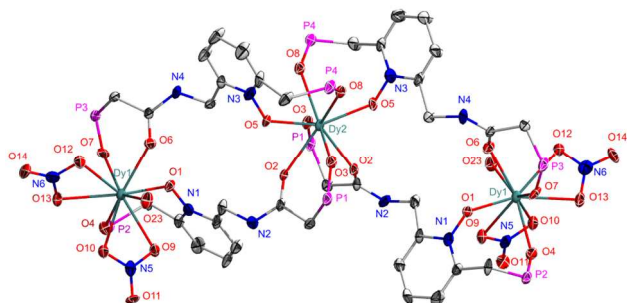


Figure 12. X-ray crystal structure for $[\text{Dy}_3(\mathbf{7})_4(\text{NO}_3)_4(\text{H}_2\text{O})_2](\text{NO}_3)_5 \cdot (\text{MeOH})_5 \cdot (\text{H}_2\text{O})_2$ (thermal ellipsoids, 50%) with atom labels, H-atoms, phenyl substituents, lattice nitrate ions, water and methanol molecules omitted for clarity. Color scheme: blue = N, red = O, lilac = P, gray = C, turquoise = Dy.

coordinate with the inner sphere positions generated by O-atoms from a bidentate NOPO fragment, Dy1-O4_P 2.332(7)Å, Dy1-O1_N 2.304(7) Å, a bidentate CMPO fragment, Dy1-O7_P 2.353(7) Å, Dy1-O6_C 2.411(7) Å, two relatively symmetric, bidentate nitrate ions and a water molecule, Dy1-O23 2.365(7) Å.

Interestingly, the crystal structure analyses for this limited set of complexes, under the preparative conditions employed so far, indicate that, despite modest ligand strain energies, neither **6** nor **7** adopt mononuclear chelate structures using the maximal denticity available. Apparently, for this to occur in the presence of nitrate counter-ions, a greater degree of structural preorganization must be built into the ligand structure. It is noted that the donor group bond lengths, X-O (X = P, N, C), as expected, lengthen slightly upon coordination relative to the

respective free ligand bond lengths although this is not the case for P2-O4 in the NOPO fragments of both complexes of **7** and the carbonyl bond length, C40-O6 in the outer components of the Dy(III) complex of **7**.

The structures observed in the complexes with **7** suggested that the coordination chemistry of its precursor pyridine derivative, **13**, was worth study. Indeed, crystallization of the 1:1 complex formed from $\text{La}(\text{NO}_3)_3 \cdot n\text{H}_2\text{O}$ and **13** from methanol solution gives single crystals with a composition $\{[\text{La}(\mathbf{13})(\text{NO}_3)_3(\text{MeOH})] \cdot (\text{MeOH})\}_n$. The complex adopts a linear chain structure as shown in Figure 13,⁴² and selected bond lengths are listed in Table 3. Each La(III) ion is ten coordinate with the coordination positions occupied by the phosphine oxide O-atom of a monodentate NPO fragment of one molecule of **13**, La1-O3_{ap} 2.411(2) Å, the two O-atoms of an appended bidentate CMPO fragment of a second molecule of **13**, La1-O2_p 2.467(2) Å, La1-O1_c 2.551(2) Å, six O-atoms from three asymmetric bidentate nitrate anions and an O-atom from an inner sphere MeOH molecule. Therefore, each molecule of **13** is bonded in a bidentate manner through its CMPO fragment to one La(III) and bridged to a second La(III) unit through the

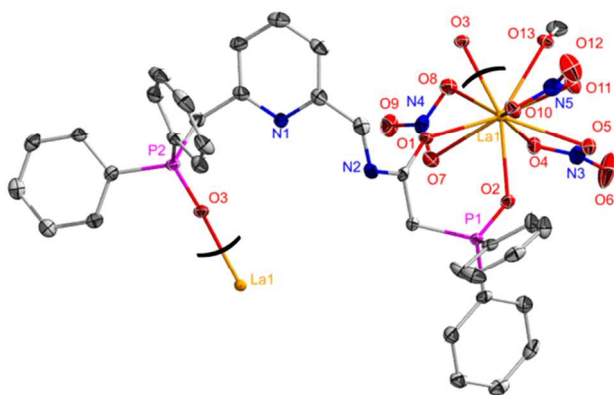


Figure 13. X-ray crystal structure and atom labeling scheme for $\{[\text{La}(\mathbf{13})(\text{NO}_3)_3(\text{MeOH})] \cdot (\text{MeOH})\}_n$ (thermal ellipsoids, 50%) with carbon atom labels, H-

atoms, and lattice methanol molecules omitted for clarity. Color scheme: blue = N, red = O, lilac = P, gray = C, yellow = La.

phosphine oxide of the NPO fragment. The pyridine N-atom is well removed from the La(III) center ($\text{La1}\cdots\text{N1a}$ 4.721(2) Å). Once again, not only does this ligand not adopt maximal $\text{O}_\text{P}\text{O}_\text{C}\text{O}_\text{P}\text{N}$ chelation, but it also does not adopt a tridentate $\text{O}_\text{P}\text{O}_\text{C}\text{O}_\text{P}$ chelate structure.

Solvent Extraction Analysis

For relevance to potential separations applications, it is preferred to perform two phase solvent extraction measurements with extractants dissolved in a hydrocarbon solvent such as dodecane. In order to achieve such solubility this usually requires that extractants of the type discussed here carry “greasy”, lipophilic substituents such as 2-ethylhexyl or octyl groups, at the least, on the phosphine oxide groups. Such compounds are accessible but usually more difficult to prepare and purify than the corresponding compounds with aryl substituents. Therefore, initial survey extractions are often accomplished with more easily prepared and purified phenyl substituted analogs that, unfortunately, are typically soluble only in less desirable chlorocarbon diluents. However, this allows for more rapid and efficient screening of extractant performance. Extractants with favorable stability and performance for trivalent f-elements in acidic aqueous solutions can then be substituent modified and subjected to additional, more detailed extraction analyses in an appropriate hydrocarbon solvent. With this point in mind, in the present study, the acid dependency for extractions of Am(III) and Eu(III) in nitric acid solutions have been initially surveyed with **6** and **7** having diphenylphosphine oxide donor groups. Distribution ratios, $D = [\text{M}_\text{org}]/[\text{M}_\text{aq}]$, were determined by using 0.01M solutions of **6** and **7** in 1,2-dichloroethane (DCE) contacted with solutions containing Eu(III) and Am(III) in aqueous nitric acid (0.01 M -5 M) at

25 °C. The variations in D values for **6**, with increasing [HNO₃] are summarized in Figure 14 and compared with extraction data for the popular, well characterized

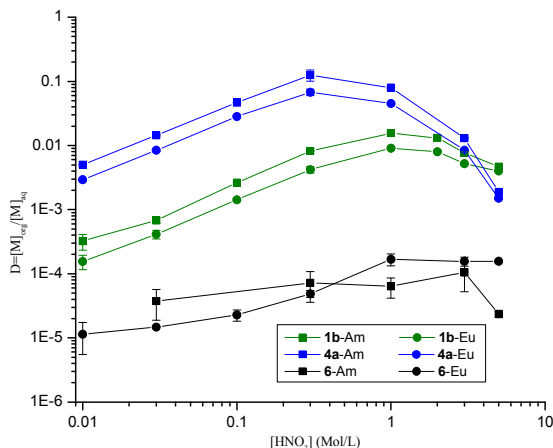


Figure 14. Eu(III) and Am(III) distribution ratios as a function of the initial nitric acid concentration. Organic phase: **6**, OPhDiBCMPO, **1b**, or DPhNOPO, **4a**, at 0.01 M in 1,2-DCE. Aqueous phase: trace ²⁴¹Am and 0.1 mM Europium nitrate in nitric acid. O/A = 1, T = 25 °C.

extractant OPhDiBCMPO, **1b** (R = Oct, R' = Ph, R'' = *i*Bu; 0.01 M) and DPhNOPO, **4a** (R = R' = Ph; 0.01 M) measured under identical conditions. Not surprisingly, as noted in our earlier studies,^{26d,27} under these conditions, the DPhNOPO ligand acts as a better extractant than OPhDiBCMPO except at the highest acid concentration (5 M).²⁷ Interestingly, the D values for **6** are unexpectedly small ($D = 10^{-4}$ or less) at all acid concentrations. This may indicate that the substitution of the N(*i*-Bu)₂ substituent on the amide group of the OPhDiBCMPO by a N(H)(CH₂C₃H₄NO) group degrades the extraction efficiency of the CMPO fragment. Alternatively, since the coordination chemistry studies show ready formation of Ln(III) complexes by **6**, the apparent weak extraction performance may reflect unfavorable aqueous phase solubility of extraction complexes containing **6** and poor phase transfer of the complexes

to the organic phase. Improved performance may be realized by appropriate substituent group modifications, and this possibility will be explored in follow-up extraction studies.

More impressive extraction behavior is found with ligand **7** (0.01 M) in DCE. The variations in D values for Eu(III) and Am(III), as a function of $[\text{HNO}_3]$, are summarized in Figure 15 along with data for DPhCMPO ($R = R' = \text{Ph}$, $R'' = \text{Et}$; 0.01 M), **1a**, DPhNOPO **4a** ($R = \text{Ph}$; 0.01 M) and TPhNOPOPO **5a** ($R = \text{Ph}$; 0.001 M). It is observed that the D values for **7** steadily increase with increasing $[\text{HNO}_3]$ from 0.10 to ~ 3 M. The unique ability to select Ln(III) and Am(III) ions over protons in these acidic solutions is similar in nature to the performance of CMPO ligands, **1**, and the NOPO and NOPOPO ligands **4** and **5**. Further, at all acid concentrations, the DCE solutions of **7** provide larger D values compared to **1a** indicating that the coupling of the NOPO fragment on the CMPO backbone through the amide N-atom leads to enhanced extractions and slightly greater selectivity for Am(III) over Eu(III). In addition, **7** displays better extraction performance compared to the parent DPhNOPO ligand **4a** at acid concentrations above 0.3 M, and it also provides slightly improved separation factors: $\text{Am}/\text{Eu} = 3.0$ (**7**), 2.0 (**1a**) and 1.8 (**4a**) at $[\text{HNO}_3] = 1$ M. On the other hand, comparisons of the extraction curve for **7** with the previously studied trifunctional TPhNOPOPO **5a**^{24h,26d,27} reveal that the D values for **7** (0.01 M in DCE) are much smaller at all acid concentrations, and the maximum D values for **7** ($D_{\text{Am}} = 0.52$, $D_{\text{Eu}} = 0.17$) appear at a lower acid concentration (~ 1 M) than observed with **5a** (0.001 M, $D_{\text{Am}} = 12$, $D_{\text{Eu}} = 10$ at 3 M $[\text{HNO}_3]$). On the other hand, the separation factor is slightly improved with **7** ($\text{SF}_{\text{Eu}}^{\text{Am}} = 3$ for **7** and ~ 1 for **5a**). In this comparison, it is very important to note that the data for **5a** in Figure 15 are for 0.001 M solutions in DCE (ten times *less* concentrated than the solution concentrations of all of the other extractants). Hence, **5a** is a significantly stronger

extractant than **7**, and replacement of one of the $-\text{CH}_2\text{P}(\text{O})\text{Ph}_2$ arms in **5a** with a N-attached CMPO fragment leads to dramatically reduced phase transfer performance.

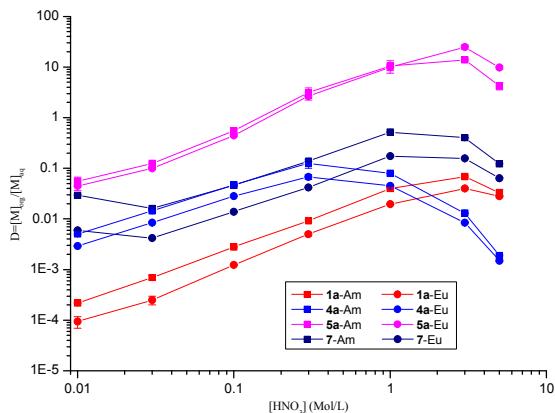
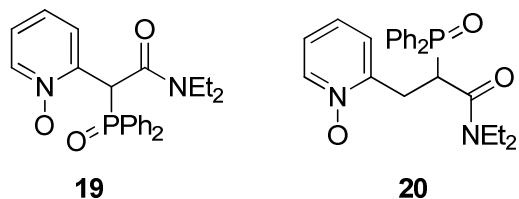


Figure 15. Eu(III) and Am(III) distribution ratios as a function of the initial nitric acid concentration. Organic phase: **7**, DPhCMPO (**1a**) or DPhNOPO (**4a**) at 0.01 M or TPhNOPOPO (**5a**) at 0.001 M⁵¹ in 1,2-DCE. Aqueous phase: trace ²⁴¹Am and 0.1 mM Europium nitrate in nitric acid. O/A = 1, T = 25 °C.

It is also instructive to compare the extraction performance of **7** with related C-attached CMPO/NOPO hybrid molecules under study in our group. For example, for the hybrid trifunctional ligands **19** and **20**, we have recently reported that **19** is a significantly more effective extractant for trivalent f-element cations than **20**.²⁷ As shown in Figure 16, **7** is a slightly stronger extractant than **19** and a much stronger extractant than **20** at all nitric acid concentrations.



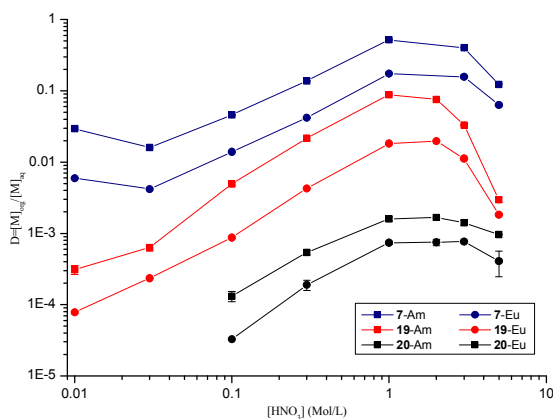


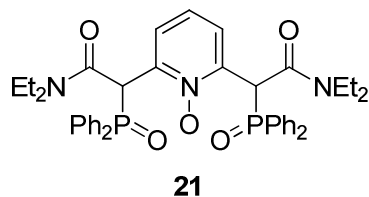
Figure 16. Eu and Am distribution ratios as a function of the initial nitric acid concentration. Organic phase: **7**, **19** or **20** at 0.01 M in 1,2-DCE. Aqueous phase: trace ^{241}Am and 0.1 mM Europium nitrate in nitric acid. O/A = 1, T = 25 °C

Lastly, it is noted that both **18** and **8** have relatively low solubility in chlorocarbon solvents, particularly in 1,2-DCE; therefore, solvent extraction analyses with these ligands are not reported. More soluble derivatives will be required to characterize the extraction performance of this framework, and the synthetic development for these compounds is in progress.

Conclusion

Syntheses for hybrid N-attached CMPO decorated pyridine N-oxide compounds **6**, **7** and **8** have been developed, and selected lanthanide coordination chemistry of the ligands has been explored. The potential lanthanide ion binding interactions for **6**, **7** and **8** have been computationally modeled in order to assess the degree of steric strain that may be encountered in forming 1:1 ligand:metal chelate structures that utilize all available O-atom donor sites in the ligands. The computed strain energetics per donor atom for **6** and **7** suggest that both ligands should be capable of forming, with modest steric hinderance, structures having maximal tridentate $\text{O}_\text{P}\text{O}_\text{C}\text{O}_\text{N}$ and tetradentate $\text{O}_\text{N}\text{O}_\text{P}\text{O}_\text{P}\text{O}_\text{C}$ chelate interactions, respectively, and the strain energetics are

closely comparable to values calculated for C-attached CMPO/NO ligands **19** and **20**.²⁷ The computed strain for pentadentate **8**, as found in the modeling for pentadentate **21**²⁷, is greater



than the values computed for **6** and **7** suggesting that the floppier ligand **8** will likely adopt chelate structures with reduced denticity. As found with C-attached CMPO pyridine N-oxide ligands **19-21**, the new N-attached CMPO pyridine N-oxide ligands **6**, **7** and **8** readily form well defined coordination complexes with Ln(NO₃)₃ salts. The preferred stoichiometry in the isolated complexes appears to be ligand:Ln = 1:1, although one 2:1 complex with **6** was obtained and structurally characterized. Spectroscopic analyses suggest that all of the ligand donor O-atoms are involved in complex formation, but in solution it is likely that the ligand:Ln interactions are asymmetric and dynamic in nature. X-ray structure analyses reveal that in crystalline complexes the ligands adopt a variety of reduced denticity chelate + bridge binding modes in which the ligand O-donor atoms compete with nitrate and solvent O-atoms for inner coordination sphere positions. This suggests that in order to achieve stronger, maximal denticity chelate interactions in the presence of competing inner sphere coordinating anions and solvents, these ligands should be modified in the organic backbone to provide a greater degree of structural preorganization. Although it is disappointing that complexes of **6** and **7** that display maximal denticity ligand binding have not been isolated and structurally characterized, this condition need not be achieved in order to obtain informative and useful extraction behavior. Preliminary measurements of the acid dependency of the solvent extraction for **6** and **7** confirm this point. The potentially tridentate ligand **6** is observed to be a surprisingly weak extractant. However, this performance

may not reflect the true solvent extraction capability of this ligand as the complexes appear to have partial solubility in the aqueous acid phase. Further substituent modifications will be required in order to perform the extractions in a more lipophilic solvent. Compound **7**, on the other hand, provides much improved performance over **6** and the parent CMPO and NOPO extractants although it is not as strongly extracting as the NOPOPO ligand, **5a**, or the bis(^CCMPO) pyridine N-oxide ligand, **21**²⁷. At this time, ligand and nitrate dependency measurements and ligand-nitric acid extraction data have not been completed for **7**, but these studies with dodecane soluble derivatives will be undertaken in the near future. The low solubility of **8** prevented extraction analysis with DCE solutions and additional derivatives with more lipophilic substituents will also require synthesis. It would be interesting to directly compare the performance of **7**, **8**, **19** and **21** with data for preorganized, multi-(N-attached CMPO) calix[4]arene ligands previously reported by Böhmer and coworkers^{16,19} and Verboom and coworkers.^{5,15,17} Unfortunately, the existing extraction measurements for these compounds have been performed under different conditions, and direct comparisons would be difficult. The studies described here suggest additional directions for extractant design, and further developments will be described in forthcoming reports.

Experimental

The organic reagents (Aldrich Chemical Co) and metal nitrates (Ventron) were used as received, and organic solvents (VWR) were dried and distilled according to standard methods. Reactions were performed under dry nitrogen unless specified otherwise. Infrared spectra were recorded on a Bruker Tensor 27 benchtop FTIR spectrometer. Solution NMR spectra were measured with Bruker Avance-300 and -500 multinuclear spectrometers using Me₄Si (¹H, ¹³C) and 85% H₃PO₄ (³¹P) as external standards. Downfield shifts from the reference resonances were given + δ values.

The atom numbering scheme for each compound is provided in the Electronic Supplementary Information (ESI). Mass spectra were obtained from the UNM Mass Spectrometry Center by using electrospray ionization with a Waters/Micromass mass spectrometer. Elemental analyses were performed by Galbraith Laboratories.

Ligand syntheses and characterization data

N-(Methylaminopyridine)chloroacetamide (**9**)

To a solution of 2-picolylamine (3.0 mL, 29 mmol) in CH₂Cl₂ (100 mL) was added (0 °C) chloroacetyl chloride (0.87 mL, 11 mmol), and the reaction mixture was stirred overnight (18 h, 23 °C). The reaction was quenched with water (50 mL), and NaHCO₃ was added until pH = 9-10. The phases were separated, and the aqueous layer was extracted with CH₂Cl₂ (3 × 50 mL). The combined organic layers were dried over MgSO₄, filtered, and concentrated in vacuo providing a golden colored oil, **9**: yield 5.04 g, 94%. ¹H NMR (300 MHz, CDCl₃):⁴⁴ δ 3.89 (s, 2H, H₈), 4.30 (d, J_{HH} = 5.7 Hz, 2H, H₆), 6.90 (dd, J_{HH} = 5.2, 7.0 Hz, 1H, H₂), 7.00 (d, J_{HH} = 7.8 Hz, 1H, H₄), 7.37 (td, J_{HH} = 1.5, 7.8 Hz, 1H, H₃), 8.23-8.28 (m, 2H, NH and H₁). ¹³C{¹H} NMR (75.4 MHz, CDCl₃):⁴⁴ δ 42.0 (C₈), 44.0 (C₆), 120.8 (C₄), 121.6 (C₂), 136.0 (C₃), 148.1 (C₁), 155.7 (C₅), 165.9 (C₇). FTIR (KBr, cm⁻¹): 3202 (ν_{NH}), 3035, 1686 (ν_{CO}), 1632, 1541, 1464, 1437, 1245, 760. HRMS (ESI): *m/z* (rel. inten., %): 185.0491 (100) [M + H⁺]. C₈H₁₀ClN₂O requires 185.0476; 207.0320 (**9**) [M + Na⁺]. C₈H₉ClN₂NaO requires 207.0296.

2-(Diphenylphosphoryl)-N-(pyridin-2-ylmethyl)acetamide (**10**)

To a solution of **9** (2.00 g, 10.8 mmol) in *o*-xylene (10 mL) was added ethyldiphenylphosphinite (4.68 mL, 21.7 mmol), and the mixture was stirred (16 h, 120 °C) under a nitrogen atmosphere. The resulting mixture was cooled (23 °C) and Et₂O (50 mL) was added. A solid formed that was

collected by filtration and washed with Et₂O (2 × 20 mL) leaving an off-white solid, **10**: yield 3.26 g, 86 %; mp 154-156 °C. ³¹P{¹H} NMR (121.5 MHz, CDCl₃): δ 30.5. ³¹P{¹H} NMR (121.5 MHz, *d*₄-MeOH): δ 32.9. ¹H NMR (300 MHz, CDCl₃): δ 3.42 (d, *J*_{HP} = 12.9 Hz, 2H, *H*₈), 4.44 (d, *J*_{HH} = 5.7 Hz, 2H, *H*₆), 6.92 (d, *J*_{HH} = 8.1 Hz, 1H, *H*₄), 7.01 (dd, *J*_{HH} = 5.1, 6.9 Hz, 1H, *H*₂), 7.35-7.47 (m, 7H, *H*_{3,11,12}), 7.67- 7.74 (m, 4H, *H*₁₀), 8.17 (t, *J*_{HH} = 5.1 Hz, 1H, *NH*), 8.40 (d, *J*_{HH} = 4.8 Hz, 1H, *H*₁). ¹H NMR (300 MHz, *d*₄-MeOH): δ 3.67 (d, *J*_{HP} = 14.1 Hz, 2H, *H*₈), 4.42 (s, 2H, *H*₆), 7.20 (d, *J*_{HH} = 7.8 Hz, 1H, *H*₄), 7.26 (dd, *J*_{HH} = 5.6 Hz, 7.1 Hz 1H, *H*₂), 7.50-7.64 (m, 6H, *H*_{11,12}), 7.79-7.86 (m, 4H, *H*₁₀), 8.17 (td, *J*_{HH} = 1.5 Hz, 7.8 Hz, 1H, *H*₃), 8.42 (d, *J*_{HH} = 4.5 Hz, 1H, *H*₁). ¹³C{¹H} NMR (75.4 MHz, CDCl₃): δ = 38.9 (d, *J*_{CP} = 60.4 Hz, *C*₈), 45.1 (*C*₆), 121.1 (*C*₄), 121.9 (*C*₂), 128.7 (d, *J*_{CP} = 12.2 Hz, *C*₁₁), 130.7 (d, *J*_{CP} = 9.9 Hz, *C*₁₀), 131.6 (d, *J*_{CP} = 102.8 Hz, *C*₉), 132.2 (d, *J*_{CP} = 2.0 Hz, *C*₁₂), 136.4 (*C*₃), 149.0 (*C*₁), 157.1 (*C*₅), 164.8 (d, *J*_{CP} = 4.4 Hz, *C*₇). FTIR (KBr, cm⁻¹): 3266 (ν_{NH}), 3064, 2968, 2916, 1668 (ν_{CO}), 1589, 1568, 1542, 1472, 1436, 1418, 1319, 1259, 1177 (ν_{PO}), 1121, 1101, 1070, 1018, 997, 879, 846, 792, 749, 724, 692, 638, 615, 574, 533, 506, 489. HRMS (ESI): *m/z* (rel. inten., %): 351.1270 (95) [M + H⁺]. C₂₀H₂₀N₂O₂P requires 351.1257; 373.1089 (100) [M + Na⁺]. C₂₀H₁₉N₂NaO₂P requires 373.1076; 389.0828 (21) [M + K⁺]. C₂₀H₁₉KN₂O₂P requires 389.0816.

2-{{2-(Diphenylphosphoryl)acetamido}methyl}pyridine 1-oxide (6)

A mixture of **10** (1.59 g, 4.54 mmol) and *m*CPBA (77 %, 1.52 g, 6.81 mmol) in CH₂Cl₂ (90 mL) was stirred (16 h, 23 °C), and the resulting mixture was quenched with an aqueous solution of NaOH (2 M, 100 mL). After separation of the phases, the organic layer was washed with aqueous NaOH solution (2 M, 2 × 50 mL), and the combined organic layers were washed with brine (100 mL), dried over MgSO₄, filtered and evaporated to dryness leaving a white solid, **6**: yield 1.08 g, 65 %; mp 152-154 °C. Anal. calcd for C₂₀H₁₉N₂O₃P·H₂O: C, 62.50; H, 5.51; N,

7.29. Found: C, 62.85; H, 5.37; N, 7.08. $^{31}\text{P}\{^1\text{H}\}$ NMR (121.5 MHz, CDCl_3): δ 29.8. $^{31}\text{P}\{^1\text{H}\}$ NMR (121.5 MHz, d_4 -MeOH): δ 32.6. ^1H NMR (500 MHz, CDCl_3): δ 3.47 (d, $J_{\text{HP}} = 13.5$ Hz, 2H, H_8), 4.51 (d, $J_{\text{HH}} = 6.0$ Hz, 2H, H_6), 6.97 (t, $J_{\text{HH}} = 7.5$ Hz, 1H, H_3), 7.02-7.06 (m, 2H, $H_{2,4}$), 7.40-7.41 (m, 4H, H_{11}), 7.48 (t, $J_{\text{HH}} = 7.5$ Hz, 2H, H_{12}), 7.72 (dd, $J_{\text{HH}} = 7.5$; 11.5 Hz, 4H, H_{10}), 8.13 (d, $J_{\text{HH}} = 6.0$ Hz, 1H, H_1), 8.37 (br, s, 1H, NH). ^1H NMR (500 MHz, d_4 -MeOH): δ 3.70 (d, $J_{\text{HP}} = 14.1$ Hz, 2H, H_8), 4.52 (s, 2H, H_6), 7.38-7.64 (m, 9H, $H_{2-4,11,12}$), 7.80-7.87 (m, 4H, H_{10}), 8.29 (d, $J_{\text{HH}} = 6.0$ Hz, 1H, H_1). $^{13}\text{C}\{^1\text{H}\}$ NMR (125.4 MHz, CDCl_3): δ 39.1 (d, $J_{\text{CP}} = 59.1$ Hz, C_8), 39.3 (C_6), 124.2 (C_2 or C_4), 124.5 (C_2 or C_4), 125.7 (C_3), 128.8 (d, $J_{\text{CP}} = 12.1$ Hz, C_{11}), 130.8 (d, $J_{\text{CP}} = 9.7$ Hz, C_{10}), 131.6 (d, $J_{\text{CP}} = 102.2$ Hz, C_9), 132.3 (C_{12}), 139.2 (C_1), 148.0 (C_5), 165.4 (C_7). FTIR (KBr, cm^{-1}): 3254 (ν_{NH}), 3055, 1669 (ν_{CO}), 1541, 1490, 1438, 1401, 1353, 1311, 1245 (ν_{NO}), 1179 (ν_{PO}), 1120, 1102, 1070, 1028, 997, 890, 851, 742, 693, 530, 500. HRMS (ESI): m/z (rel. inten., %): 367.1212 (72) [$\text{M} + \text{H}^+$]. $\text{C}_{20}\text{H}_{20}\text{N}_2\text{O}_3\text{P}$ requires 367.1206; 389.1028 (100) [$\text{M} + \text{Na}^+$]. $\text{C}_{20}\text{H}_{19}\text{N}_2\text{NaO}_3\text{P}$ requires 389.1026; 755.2154 (34) [$2\text{M} + \text{Na}^+$]. $\text{C}_{40}\text{H}_{38}\text{N}_4\text{NaO}_6\text{P}_2$ requires 755.2164. Soluble: CH_2Cl_2 , CHCl_3 and MeOH. Insoluble: MeCN, EtOAc, THF, hexane and toluene.

2-chloro-N- $\{6$ -((diphenylphosphoryl)methyl)pyridin-2-yl $\}$ methylacetamide (**12**)

To a mixture of **11** (3.44 g, 10.7 mmol) and triethylamine (3.0 mL, 21 mmol) in CH_2Cl_2 (60 mL) was added (0 °C) chloroacetyl chloride (1.02 mL, 12.8 mmol), and the mixture was stirred (15 min, 0 °C). The resulting reddish solution was then warmed and stirred (16 h, 23 °C). Water (100 mL) was added, and the aqueous layer was extracted with CH_2Cl_2 (3 \times 80 mL). The combined organic layers were washed with brine solution, dried (MgSO_4), filtered, and the filtrate concentrated in vacuo. Purification by flash chromatography on silica gel (eluent: CH_2Cl_2 / MeOH, 98:2 to 95:5) afforded a yellow foam that solidified upon standing (23 °C), **12**: yield 3.02

g, 71 %; mp 144-146 °C. $^{31}\text{P}\{^1\text{H}\}$ NMR (121.5 MHz, CDCl_3): δ 30.3. ^1H NMR (300 MHz, CDCl_3): δ 3.78 (d, $J_{\text{HP}} = 14.1$ Hz, 2H, H_7), 3.94 (s, 2H, H_{13}), 4.26 (d, $J_{\text{HH}} = 5.1$ Hz, 2H, H_1), 6.87 (d, $J_{\text{HH}} = 7.8$ Hz, 1H, H_3 or H_5), 7.14 (d, $J_{\text{HH}} = 7.5$ Hz, 1H, H_3 or H_5), 7.26-7.37 (m, 7H, $H_{4,10,11}$), 7.61 (dd, $J_{\text{HH}} = 6.9$; 11.7 Hz, 4H, H_9), 8.22 (t, $J_{\text{HH}} = 4.5$ Hz, 1H, NH). $^{13}\text{C}\{^1\text{H}\}$ NMR (75.4 MHz, CDCl_3): δ 39.5 (d, $J_{\text{CP}} = 64.0$ Hz, C_7), 42.4 (C_{13}), 44.0 (C_1), 119.4 (C_3 or C_5), 123.3 (d, $J_{\text{CP}} = 3.2$ Hz, C_3 or C_5), 128.2 (d, $J_{\text{CP}} = 11.8$ Hz, C_{10}), 130.8 (d, $J_{\text{CP}} = 9.4$ Hz, C_9), 131.6 (C_{11}), 132.0 (d, $J_{\text{CP}} = 99.8$ Hz, C_8), 136.9 (C_4), 151.6 (d, $J_{\text{CP}} = 7.4$ Hz, C_6), 155.0 (C_2), 165.7 (C_{12}). FTIR (KBr, cm^{-1}): 3243 (ν_{NH}), 3064, 1673 (ν_{CO}), 1586, 1572, 1484, 1455, 1439, 1398, 1345, 1317, 1284, 1247, 1230, 1178 (ν_{PO}), 1157, 1122, 1100, 1072, 1027, 991, 934, 839, 813, 763, 745, 714, 692, 649, 601, 520, 497, 480. HRMS (ESI): m/z (rel. inten., %): 399.1019 (48) [$\text{M} + \text{H}^+$]. $\text{C}_{21}\text{H}_{21}\text{ClN}_2\text{O}_2\text{P}$ requires 399.1024; 421.0842 (100) [$\text{M} + \text{Na}^+$]. $\text{C}_{21}\text{H}_{20}\text{ClN}_2\text{NaO}_2\text{P}$ requires 421.0843.

2-(Diphenylphosphoryl)-N-{{6-((diphenylphosphoryl)methyl)pyridin-2-yl}methyl}acetamide (13)

To a solution of **12** (3.02 g, 7.57 mmol) in *o*-xylene (15 mL) was added ethyldiphenylphosphinite (3.3 mL, 15 mmol), and the mixture was stirred (16 h, 120 °C) under a nitrogen atmosphere. The resulting green mixture was cooled (23 °C), the resulting solid was collected by filtration, rinsed with hexane (2×20 mL) and dried in air (12 h) leaving an off-white solid, **13**: yield 4.16 g, 97%; mp 172-174 °C. $^{31}\text{P}\{^1\text{H}\}$ NMR (121.5 MHz, CDCl_3): δ 29.7 ($\text{PCH}_2\text{C}(\text{O})$), 30.7 (PCH_2Py). $^{31}\text{P}\{^1\text{H}\}$ NMR (121.5 MHz, d_4 -MeOH): δ 32.7 ($\text{PCH}_2\text{C}(\text{O})$), 34.6 (PCH_2Py). ^1H NMR (500 MHz, CDCl_3): δ 3.39 (d, $J_{\text{HP}} = 13.0$ Hz, 2H, H_{13}), 3.87 (d, $J_{\text{HH}} = 14.5$ Hz, 2H, H_7), 4.32 (d, $J_{\text{HH}} = 5.5$ Hz, 2H, H_1), 6.73 (d, $J_{\text{HH}} = 7.5$ Hz, 1H, H_3 or H_5), 7.25 (d, $J_{\text{HH}} = 7.5$ Hz, 1H, H_3 or H_5), 7.32 (t, $J_{\text{HH}} = 7.5$ Hz, 1H, H_4), 7.40-7.46 (m, 10H, $H_{10,11,16}$), 7.52 (t, $J_{\text{HH}} =$

7.0 Hz, 2H, H_{17}), 7.70 (dd, $J_{\text{HH}} = 8.0$; 11.0 Hz, 8H, $H_{9,15}$), 7.96 (br, s, 1H, NH). ^1H NMR (500 MHz, d_4 -MeOH): δ 3.63 (d, $J_{\text{HP}} = 14.4$ Hz, 2H, H_{13}), 4.05 (d, $J_{\text{HP}} = 14.1$ Hz, 2H, H_7), 4.25 (s, 2H, H_1), 6.97 (d, $J_{\text{HH}} = 7.8$ Hz, 1H, H_3 or H_5), 7.10 (d, $J_{\text{HH}} = 7.5$ Hz, 1H, H_3 or H_5), 7.48-7.67 (m, 13H, $H_{4,10,11,16,17}$), 7.74-7.85 (m, 8H, $H_{9,15}$). $^{13}\text{C}\{^1\text{H}\}$ NMR (125.4 MHz, CDCl_3): δ 38.9 (d, $J_{\text{CP}} = 60.0$ Hz, C_{13}), 40.7 (d, $J_{\text{CP}} = 64.1$ Hz, C_7), 44.9 (C_1), 119.1 (C_3 or C_5), 123.2 (C_3 or C_5), 128.4 (d, $J_{\text{CP}} = 11.7$ Hz, C_{10} or C_{16}), 128.9 (d, $J_{\text{CP}} = 12.1$ Hz, C_{10} or C_{16}), 130.8 (d, $J_{\text{CP}} = 9.7$ Hz, C_9 or C_{15}), 131.2 (d, $J_{\text{CP}} = 9.4$ Hz, C_9 or C_{15}), 131.7 (d, $J_{\text{CP}} = 107.1$ Hz, C_{14}), 131.8 (C_{11} or C_{17}), 132.4 (C_{11} or C_{17}), 132.4 (d, $J_{\text{CP}} = 99.8$ Hz, C_8), 137.0 (C_4), 151.9 (d, $J_{\text{CP}} = 6.9$ Hz, C_6), 156.4 (C_2), 164.7 (d, $J_{\text{CP}} = 3.9$ Hz, C_{12}). FTIR (KBr, cm^{-1}): 3282 (ν_{NH}), 3055, 2962, 2909, 1672 (ν_{CO}), 1591, 1574, 1539, 1484, 1454, 1436, 1417, 1313, 1266, 1178 (ν_{PO}), 1120, 1104, 1069, 1026, 996, 880, 835, 804, 747, 721, 693, 610, 579, 516, 479. HRMS (ESI) m/z (rel. inten., %): 565.1800 (44) [$\text{M} + \text{H}^+$]. $\text{C}_{33}\text{H}_{31}\text{N}_2\text{O}_3\text{P}_2$ requires 565.1804; 587.1626 (100) [$\text{M} + \text{Na}^+$]. $\text{C}_{33}\text{H}_{30}\text{N}_2\text{NaO}_3\text{P}_2$ requires 587.1624; 603.1339 (15) [$\text{M} + \text{K}^+$]. $\text{C}_{33}\text{H}_{30}\text{KN}_2\text{O}_3\text{P}_2$ requires 603.1363.

2-**{[2-(Diphenylphosphoryl)acetamido]methyl}**-6-**[(diphenylphosphoryl)methyl]pyridine 1-oxide (7)**

A mixture of **13** (3.56 g, 6.31 mmol) and *m*CPBA (77 %, 2.1 g, 9.45 mmol) in CH_2Cl_2 (130 mL) was stirred (18 h, 23 °C), and the resulting mixture was quenched with an aqueous solution of KOH (2 M, 100 mL). After separation of the phases, the organic layer was washed with an aqueous solution of KOH (2 M, 2 × 40 mL), and the combined organic layers were washed with brine solution (80 mL), dried (MgSO_4), filtered and evaporated to dryness leaving a yellow powder, **7**: yield 2.4 g, 67 %; mp 222-224 °C. Anal. calcd. for $\text{C}_{33}\text{H}_{30}\text{N}_2\text{O}_4\text{P}_2$: C, 68.27; H, 5.21; N, 4.83. Found: C, 67.20; H, 5.27; N, 4.62. $^{31}\text{P}\{^1\text{H}\}$ NMR (121.5 MHz, CDCl_3): δ 29.4 ($P\text{CH}_2\text{C}(\text{O})$), 31.4 ($P\text{CH}_2\text{Py}$). $^{31}\text{P}\{^1\text{H}\}$ NMR (121.5 MHz, d_4 -MeOH): δ 32.8 ($P\text{CH}_2\text{C}(\text{O})$), 34.4

(PCH₂Py). ¹H NMR (500 MHz, CDCl₃): δ 3.38 (d, *J*_{HP} = 13.0 Hz, 2H, *H*₁₃), 4.16 (d, *J*_{HP} = 13.5 Hz, 2H, *H*₇), 4.39 (d, *J*_{HH} = 6.0 Hz, 2H, *H*₁), 6.73 (d, *J*_{HH} = 7.5 Hz, 1H, *H*₃), 6.80 (t, *J*_{HH} = 7.5 Hz, 1H, *H*₄), 7.26-7.40 (m, 10H, *H*_{10,11,16}), 7.49 (t, *J*_{HH} = 7.0 Hz, 2H, *H*₁₇), 7.58 (d, *J*_{HH} = 7.5 Hz, 1H, *H*₅), 7.70 (dd, *J*_{HH} = 8.0, 11.5 Hz, 4H, *H*₉ or *H*₁₅), 7.76 (dd, *J*_{HH} = 8.0, 11.0 Hz, 4H, *H*₉ or *H*₁₅), 8.08 (br s, 1H, NH). ¹H NMR (500 MHz, *d*₄-MeOH): δ 3.65 (d, *J*_{HP} = 14.1 Hz, 1H, *H*₁₃), 4.35 (d, *J*_{HP} = 14.1 Hz, 2H, *H*₇), 4.35 (s, 2H, *H*₁), 7.16-7.27 (m, 2H, *H*_{3,4}), 7.44-7.64 (m, 13H, *H*_{5,10,11,16,17}), 7.77-7.85 (m, 8H, *H*_{9,15}). ¹³C {¹H} NMR (125 MHz, CDCl₃): δ 31.1 (d, *J*_{CP} = 66.4 Hz, *C*₇), 39.0 (d, *J*_{CP} = 59.5 Hz, *C*₁₃), 39.7 (*C*₁), 122.3 (*C*₃), 124.6 (*C*₄), 125.7 (*C*₅), 128.5 (d, *J*_{CP} = 12.0 Hz, *C*₁₀ or *C*₁₆), 128.9 (d, *J*_{CP} = 12.1 Hz, *C*₁₀ or *C*₁₆), 130.8 (d, *J*_{CP} = 8.6 Hz, *C*_{9,15}), 131.5 (d, *J*_{CP} = 102.4 Hz, *C*₁₄), 131.9 (d, *J*_{CP} = 101.2 Hz, *C*₈), 132.1 (*C*₁₁ or *C*₁₇), 132.4 (*C*₁₁ or *C*₁₇), 143.7 (d, *J*_{CP} = 4.0 Hz, *C*₆), 165.2 (d, *J*_{CP} = 4.5 Hz, *C*₁₂). FTIR (KBr, cm⁻¹): 3250 (ν_{NH}), 3056, 2863, 1673 (ν_{CO}), 1589, 1554, 1493, 1437, 1427, 1406, 1351, 1293, 1246 (ν_{NO}), 1198 (ν_{PO}), 1173 (ν_{PO}), 1119, 1105, 1072, 1036, 996, 936, 881, 849, 830, 774, 722, 697, 587, 553, 520, 503, 459. HRMS (ESI) *m/z* (rel. inten., %): 581.1750 (12) [M + H⁺]. C₃₃H₃₁N₂O₄P₂ requires 581.1754; 603.1577 (100) [M + Na⁺]. C₃₃H₃₀N₂NaO₄P₂ requires 603.1573. Soluble: CH₂Cl₂, CHCl₃, MeOH and toluene. Insoluble: Et₂O, MeCN, EtOAc, THF, hexane.

2,6-Bis(azidomethyl)pyridine (15)

To a mixture of 2,6-bis(chloromethyl)pyridine, **14**^{24h} (5.0 g, 28 mmol), 18-crown-6 (catalytic amount) and tetrabutylammonium bromide (catalytic amount) in DMF (10 mL) was added, with caution, sodium azide (4.6 g, 71 mmol). The resulting solution was stirred (17 h, 23 °C), and EtOAc (100 mL) was added. The organic layer was washed with an aqueous solution of NaHCO₃ (2 M, 100 mL), and the organic phase was separated, dried (MgSO₄), filtered, and concentrated in vacuo to afford an orange liquid, **15**: yield 5.03 g, 94%. ¹H NMR (300 MHz,

CDCl₃): δ 4.43 (s, 4H, *H*₁), 7.25 (d, *J*_{HH} = 7.8 Hz, 2H, *H*₃), 7.70 (t, *J*_{HH} = 7.8 Hz, 1H, *H*₄).
¹³C{¹H} NMR (75.4 MHz, CDCl₃): δ 54.8 (*C*₁), 120.6 (*C*₃), 137.5 (*C*₄), 155.5 (*C*₂).

Pyridine-2,6-diylldimethanamine (16)

To a solution of **15** (1.0 g, 5.3 mmol) in ethanol (100 mL) was added, in portions, palladium on carbon (10%, 107 mg). The solution was purged three times with hydrogen (1 atm), and the solution was stirred under a static hydrogen atmosphere (2 atm, 3 h). The solution was filtered over a pad of Celite, rinsed with EtOH (30 mL) and evaporated leaving an orange oil, **16**: yield 655 mg, 90%. ¹H NMR (300 MHz, CDCl₃) δ 1.32 (s, 2H, *NH*₂), 3.54 (s, 4H, *H*₁), 6.75 (d, *J*_{HH} = 7.8 Hz, 1H, *H*₄), 7.21 (t, *J*_{HH} = 7.8 Hz, 1H, *H*₃). ¹³C{¹H} NMR (75.4 MHz, CDCl₃): δ 46.9 (*C*₁), 118.3 (*C*₃), 136.2 (*C*₄), 160.7 (*C*₂). FTIR (KBr, cm⁻¹): 3313, 3252, 2924, 1593, 1575, 1456, 1396, 1373, 1309, 1214, 1157, 1083, 1034, 992, 929, 790, 756, 712, 530. HRMS (ESI) *m/z* (rel. inten., %): 138.1026 [*M* + *H*⁺] (100). C₇H₁₂N₃ requires 138.1026; 160.0852 [*M* + Na⁺] (13). C₇H₁₁N₃Na requires 160.0845.

N,N'-(Pyridine-2,6-diylbis(methylene))bis(2-chloroacetamide) (17)

To a solution of chloroacetyl chloride (1.16 mL, 14.6 mmol) in CH₂Cl₂ (15 mL), **16** (1.00 g, 7.29 mmol) was added dropwise with stirring (0°C). Stirring was continued (15 min, 0°C), and the resulting yellow solution was then stirred (23 °C, 16 h). A saturated NaHCO₃ solution (50 mL) was added, and the aqueous layer was extracted with CH₂Cl₂ (3 × 30 mL). The combined organic layers were washed with aqueous brine solution, dried (MgSO₄), filtered and the filtrate concentrated in vacuo leaving an orange oil, **17**: yield 1.44 g, 68 %. ¹H NMR (300 MHz, CDCl₃): δ 4.07 (s, 2H, *H*₆), 4.55 (d, *J*_{HH} = 5.1 Hz, 4H, *H*₁), 7.13 (d, *J*_{HH} = 7.5 Hz, 2H, *H*₃), 7.62 (t, *J*_{HH} = 7.8 Hz, 1H, *H*₄), 7.77 (br s, 2H, *NH*). ¹³C{¹H} NMR (75.4 MHz, CDCl₃): δ 42.7 (*C*₁), 44.4 (*C*₆),

120.6 (C_3), 137.8 (C_4), 155.4 (C_2), 166.1 (C_5). HRMS (ESI) m/z (rel. inten., %): 290.0463 [$M + H^+$] (100). $C_{11}H_{14}Cl_2N_3O_2$ requires 290.0463; 312.0279 [$M + Na^+$] (40). $C_{11}H_{13}Cl_2N_3NaO_2$ requires 312.0283; 328.0024 [$M + K^+$] (23). $C_{11}H_{13}Cl_2KN_3O_2$ requires 328.0022.

N,N'-(pyridine-2,6-diylbis(methylene))bis(2-(diphenylphosphoryl)acetamide) (18)

To a solution of **16** (0.50 g, 3.6 mmol) and K_2CO_3 (5.30 g, 38.2 mmol) in CH_2Cl_2 (100 mL) was added chloroacetyl chloride (2.90 mL, 36.40 mmol) (0 °C) followed by slow addition of water (0.65 mL, 36.40 mmol) (2 h, 0 °C). The mixture was stirred (16 h, 23 °C), and was subsequently filtered, and the filtrate was evaporated to dryness. Ethyl diphenylphosphite (7.90 mL, 36.4 mmol) was added to the resulting oil, and the mixture was stirred and heated (120 °C, 16 h). The mixture was cooled (23 °C) and Et_2O (100 mL) was added. The precipitate was recovered by filtration, rinsed with Et_2O (2 × 20 mL), and dried in air (4 h) leaving an off-white solid. Subsequently, the crude solid was dissolved in CH_2Cl_2 , and slow evaporation of this solution afforded white needles, **18**: yield 2.05 g, 91%; mp 226-228 °C. Anal. calcd. for $C_{35}H_{33}N_3O_4P_2 \cdot 3H_2O$: C, 62.22; H, 5.82; N 6.22. Found: C, 61.83; H, 5.38; N, 6.26. $^{31}P\{^1H\}$ (121.5 MHz, $CDCl_3/d_4$ -MeOH): δ 32.4. 1H NMR (300 MHz, $CDCl_3/d_4$ -MeOH): δ 3.57 (d, $J_{HH} = 14.1$ Hz, 4H, H_6), 4.43 (br s, 4H, H_1), 6.99 (d, $J_{HH} = 7.8$ Hz, 2H, H_3), 7.36-7.54 (m, 13H, $H_{4,9,10}$), 7.64-7.71 (m, 8H, H_8), 8.67 (t, $J_{HH} = 4.2$ Hz, 2H, NH_2). $^{13}C\{^1H\}$ NMR (75.4 MHz, $CDCl_3/d_4$ -MeOH): δ 39.0 (d, $J_{CP} = 62.2$ Hz, C_6), 44.7 (C_1), 120.4 (C_3), 129.2 (d, $J_{CP} = 12.4$ Hz, C_9), 131.2 (d, $J_{CP} = 10.1$ Hz, C_8), 131.3 (d, $J_{CP} = 103.9$ Hz, C_7), 132.9 (d, $J_{CP} = 2.0$ Hz, C_{10}), 138.0 (C_4), 155.7 (C_2), 165.8 (d, $J_{CP} = 4.7$ Hz, C_5). FTIR (KBr, cm^{-1}) 3262 (ν_{NH}), 3058, 2968, 2914, 1673 ($\nu_{C=O}$), 1596, 1578, 1545, 1484, 1458, 1437, 1415, 1402, 1309, 1180 ($\nu_{P=O}$), 1120, 1102, 1069, 1026, 910, 888, 843, 745, 692, 587, 528, 507. HRMS (ESI) m/z (rel. inten., %): 622.2022 [$M +$

H^+] (29). $C_{35}H_{34}N_3O_4P_2$ requires 622.2019; 644.1847 [$M + Na^+$] (100). $C_{35}H_{33}N_3NaO_4P_2$ requires 644.1839; 660.1562 [$M+K^+$] (8). $C_{35}H_{33}KN_3O_4P_2$ requires 660.1578.

2,6-Bis{[2-(diphenylphosphoryl)acetamido]methyl}pyridine 1-oxide (8)

A mixture of **18** (1.1 g, 1.8 mmol) and *m*CPBA (77 %, 0.65 g, 2.7 mmol) in CH_2Cl_2 (250 mL) was stirred overnight (18 h, 23 °C). The resulting mixture was quenched with an aqueous solution of KOH (2 M, 50 mL), the phases separated, and the organic layer was washed with an aqueous solution of KOH (2 M, 2 × 50 mL). The combined organic layers were washed with aqueous brine solution (80 mL), dried ($MgSO_4$), filtered and the filtrate evaporated until ~ 50 mL remained. Et_2O (100 mL) was added, and the subsequent precipitate was filtered and dried in air, leaving a white solid, **8**: yield 0.788 g, 69 %; mp 222-224 °C. $^{31}P\{^1H\}$ (121.5 MHz, $CDCl_3/d_4$ -MeOH): δ 32.4. $^{31}P\{^1H\}$ (121.5 MHz, d_4 -MeOH): δ 32.5. 1H NMR (300 MHz, $CDCl_3/d_4$ -MeOH): δ 3.54 (d, $J_{HP} = 13.2$ Hz, 4H, H_6), 4.41 (s, 4H, H_1), 6.90 (m, 2H, H_3), 7.36-7.53 (m, 13H, $H_{4,9,10}$), 7.68-7.74 (m, 8H, H_8). 1H NMR (300 MHz, d_4 -MeOH): δ 3.68 (d, $J_{HP} = 14.1$ Hz, 4H, H_6), 4.49 (s, 4H, H_1), 6.88-7.98 (m, H_{aryl}). $^{13}C\{^1H\}$ NMR (75.4 MHz, $CDCl_3/d_4$ -MeOH): δ 38.3 (d, $J_{CP} = 62.7$ Hz, C_6), 38.9 (C_1), 123.1 (C_3), 126.8 (C_4), 128.8 (d, $J_{CP} = 12.4$ Hz, C_9), 130.2 (d, $J_{CP} = 95.2$ Hz, C_7), 130.7 (d, $J_{CP} = 10.2$ Hz, C_8), 132.6 (C_{10}), 147.6 (C_2), 166.0 (C_5). FTIR (KBr, cm^{-1}): 3263 (ν_{NH}), 3056, 1674 ($\nu_{C=O}$), 1590, 1537, 1437, 1295, 1248 (ν_{N-O}), 1185 ($\nu_{P=O}$), 1122, 1103, 1071, 1028, 998, 844, 749, 726, 695, 523. HRMS (ESI) m/z (rel. inten., %): 638.1987 [$M + H^+$] (6). $C_{35}H_{34}N_3O_5P_2$ requires 638.1968; 660.1802 [$M + Na^+$] (100). $C_{35}H_{33}N_3NaO_5P_2$ requires 660.1788;

Lanthanide Coordination Complexes.

The lanthanide nitrate/ligand complexes were generally obtained from the addition of equimolar amounts (1 mmol) of a hydrated metal nitrate (La, Pr, Eu, Dy, Er, Yb, Lu) in MeOH (10 mL) to **6**, **7**, **13** and **18** in MeOH (10 mL). The mixtures were stirred (2 h, 23 °C), filtered and the filtrates evaporated to dryness leaving crude powders that were crystallized from MeOH or mixed solvent combinations. In general, CHN analyses were not in agreement with solvent-free compositions, and in many cases lattice solvent molecules were easily lost during sample handling. Key infrared spectral data for powder samples of the complexes used to obtain single crystals for X-ray diffraction analysis are summarized below. Additional data are included in the Electronic Supplementary Information (ESI, Table S.70). [Er(**6**)₂(H₂O)₂](NO₃)₃, pink powder: FTIR (KBr, cm⁻¹): 1637 (ν_{C=O}), 1237 (ν_{N-O}), 1165 (ν_{P=O}). [Yb(**6**)(NO₃)₃], colorless powder: FTIR (KBr, cm⁻¹): 1634 (ν_{C=O}), 1229 (ν_{N-O}), 1160 (ν_{P=O}). [Eu(**7**)(NO₃)₃], white powder: FTIR (KBr, cm⁻¹): 1635 (ν_{C=O}), 1211 (ν_{N-O}), 1159 (ν_{P=O}). [Dy(**7**)(NO₃)₃], colorless powder: FTIR (KBr, cm⁻¹): 1642 (ν_{C=O}), 1231, 1215 (ν_{N-O}), 1160 (ν_{P=O}). [La(**13**)(NO₃)₃], colorless powder: FTIR (KBr, cm⁻¹): 1630 (ν_{C=O}), 1154 (ν_{P=O}). Single crystals of selected complexes were obtained by slow evaporation of a concentrated solution of the complexes.

X-ray Diffraction Analyses.

Single crystals were coated with Paratone oil, and each was mounted on a CryoLoop attached to a metal pin with epoxy. Diffraction data were collected with a Bruker X8 Apex II CCD-based X-ray diffractometer that was equipped with an Oxford Cryostream 700 low temperature device and normal focus Mo-target X-ray tube ($\lambda = 0.71073 \text{ \AA}$) operated at 1500 W power (50 kV, 30 mA). Data collection and processing were performed with the Bruker APEX2 software suite.⁴⁵ Structures were solved by direct methods and refined with full-matrix least-squares methods on

F^2 with use of SHELXTL.⁴⁶ Lattice and data collection parameters for the ligands and the metal complexes are presented in Tables 1 and 2, respectively. Unless otherwise indicated below, all heavy atoms were refined anisotropically and C-H hydrogen atoms were included in idealized positions and refined isotropically (riding model) with $U_{iso} = 1.2 U_{eq}$ of the parent atom ($U_{iso} = 1.5 U_{eq}$ for methyl H-atoms). The N-H and O-H hydrogen atoms were located in the diffraction map and were refined with $U_{iso} = 1.5 U_{eq}$ of the parent atom for all structures except $\{[\text{La}(\mathbf{13})(\text{NO}_3)_3(\text{MeOH})] \cdot (\text{MeOH})\}_n$, $\{[\text{Eu}(\mathbf{7})(\text{NO}_3)_2(\text{EtOAc})_{0.5}(\text{H}_2\text{O})_{0.5}](\text{NO}_3)_2 \cdot (\text{MeOH})\}_n$, and $[\text{Dy}_3(\mathbf{7})_4(\text{NO}_3)_4(\text{H}_2\text{O})_2](\text{NO}_3)_5 \cdot (\text{MeOH})_5 \cdot (\text{H}_2\text{O})_2$. The structure refinements were well behaved except as indicated in the following notes. $\mathbf{6} \cdot 2\text{H}_2\text{O}$, colorless blocks obtained by slow evaporation of a hydrated sample from a mixture of methanol/acetone (1:1) in an open vial. $\mathbf{7}$, colorless blocks obtained by slow evaporation of a sample of $\mathbf{7}$ from MeOH/Et₂O. $\mathbf{12}$, colorless blocks obtained by slow evaporation of a sample of $\mathbf{12}$ from CH₂Cl₂. $\mathbf{18} \cdot \text{CH}_3\text{OH}$, colorless rods obtained by slow evaporation of a solution of the compound used for CHN analysis from CH₂Cl₂; the lattice methanol sits on a special position with three crystallographic symmetry elements passing through O3. $\{[\text{Yb}(\mathbf{6})(\text{NO}_3)_3] \cdot (\text{MeOH})\}_n$, colorless plates. $\{[\text{Lu}(\mathbf{6})(\text{NO}_3)_3] \cdot (\text{MeOH})\}_n$, colorless prisms. $[\text{Er}(\mathbf{6})_2(\text{H}_2\text{O})_2](\text{NO}_3)_3 \cdot (\text{H}_2\text{O})_4\}_n$, pink rods. $\{[\text{La}(\mathbf{13})(\text{NO}_3)_3(\text{MeOH})] \cdot (\text{MeOH})\}_n$, colorless block., $\{[\text{Eu}(\mathbf{7})(\text{NO}_3)_2(\text{EtOAc})_{0.5}(\text{H}_2\text{O})_{0.5}](\text{NO}_3)_2 \cdot (\text{MeOH})\}_n$, colorless prisms; disordered solvent molecules were found coordinated to the Eu ion and modeled as 50 % EtOAc and 50 % H₂O with a hydrogen-bonded MeOH. Additional disordered solvent was accounted for by using SQUEEZE⁴⁷ which found voids of 263 Å³ containing 104 electrons. $[\text{Dy}_3(\mathbf{7})_4(\text{NO}_3)_4(\text{H}_2\text{O})_2](\text{NO}_3)_5 \cdot (\text{MeOH})_5 \cdot (\text{H}_2\text{O})_2$ colorless blocks; One O-atom in a poorly behaved solvent water molecule was treated isotropically. The relative occupancies of the O-

atoms on one disordered nitrate were freely refined. The occupancy of the MeOH solvent was approximated with use of a free variable and then set to 50 %. Additional solvent that could not be adequately modeled was accounted for by using SQUEEZE⁴⁷ which revealed voids of 616 Å³ containing 239 electrons.

[Insert Table 1 and Table 2 near here]

Photophysical Characterization

Solutions for photophysical characterization were prepared in a glovebox with controlled nitrogen atmosphere ($O_2 < 0.5$ ppm, $H_2O < 1$ ppm). Samples of [Eu(**6**)(NO₃)₃] and [Eu(**7**)(NO₃)₃] (approximately 20 mg) were initially dissolved in methanol (3 mL) and stirred (15 min). After measurement in methanol, the solvent was evaporated, and the sample was re-dissolved in deuterated methanol (5 mL) for additional spectroscopic measurements. Solutions were equilibrated for at least two days before measurements were made. The emission spectra and lifetimes were measured on a Jobin-Yvon Fluorolog-3 spectrofluorimeter equipped with a red-sensitive PMT R928 detector and a Xe flash lamp. The excitation wavelengths were 284 and 275 nm, for the complexes with **6** and **7**, respectively, and emission and excitation slits were $2 \leq \text{slit width} \leq 5$ nm for the spectra and for the lifetime measurements. The lifetime measurements were performed using the Horiba DataStation software control. The number of coordinated methanol molecules n_{MeOH} was determined through comparison of the emission lifetimes of Eu(III) in methanol and deuterated methanol, using the equation $n_{\text{MeOH}} = 2.1(\tau_{\text{MeOH}}^{-1} - \tau_{\text{MeOD}}^{-1})$ proposed by Horrocks and Sudnick.⁴¹ All reported lifetimes are the average of at least three independent measurements.

Distribution Measurements

All salts and solvents were reagent grade and were used as received. Extraction experiments were performed using 1,2-dichloroethane (OmniSolv, EM Science) as the extractant diluent. The aqueous phases were prepared using nitric acid (J. T. Baker, Ultrex II) and europium nitrate (Aldrich, 99.9%). Distilled, deionized water was obtained from a Barnstead Nanopure filter system (resistivity at least 18.2 M Ω -cm) and used to prepare all the aqueous solutions. The americium radioisotope, ^{241}Am , was obtained from the Radiochemical and Engineering Research Center (REDC) at ORNL. The radiotracer $^{152/154}\text{Eu}$ was purchased from Isotope Products, Burbank, CA. Both were added as spikes to the aqueous phases in the sample equilibration vials in the extraction experiments.

The organic and aqueous phases (1:1 organic to aqueous (O:A) phase ratio) were combined in 2 mL polypropylene micro-tubes, which were capped and mounted by clips on a disk that was rotated in a constant-temperature air box at 25.0 ± 0.5 °C for 1 hour. This contacting period was chosen by determining that equilibrium was reached after a five minute contact between organic and aqueous phases. One hour contacts ensured not only that equilibrium was reached but also that the phases were at the desired temperature. The tubes were centrifuged (5 min at 3000 RPM, 25 °C) in a Beckman CoulterTM Allegra 6R temperature-controlled centrifuge. An aliquot (250 μL) of each phase was sampled and counted by using a Canberra Analyst pure Ge Gamma counter. Counting times were sufficient to ensure that counting error was a small fraction of the precision of the measured distribution ratios, as affected by a combination of volumetric, replicate and counting errors estimated to be $\pm 5\%$. Distribution ratios were calculated as the ratio of the volumetric count rates of the ^{241}Am and $^{152/154}\text{Eu}$ isotopes in each phase at equilibrium.

Molecular Mechanics Calculations

Geometry optimizations of the free and metal-bound forms of **6**, **7**, **8** and **18** were carried out with the MM3 force field⁴⁸ using a points-on-a-sphere metal ion⁴⁹ as implemented in PCModel software.⁵⁰ Conformational searches to locate the most stable form for each structure were performed using the GMMX algorithm provided with this software. Input files required to repeat these calculations including additional parameters for treating the metal-dependent interactions, are provided in the ESI.

Acknowledgments

Financial support for this study at the University of New Mexico was provided by the Division of Chemical Sciences, Geosciences and Biosciences, Office of Basic Energy Sciences, U. S. Department of Energy (Grant DE-FG02-03ER15419 (R.T.P)). In addition, funds from the National Science Foundation assisted with the purchases of the X-ray diffractometer (CHE-0443580) and NMR spectrometers (CHE-0840523 and -0946690). B.P.H. and L.H.D. acknowledge support from the Division of Chemical Sciences, Geosciences and Biosciences, Office of Basic Energy Sciences, U. S. Department of Energy. AdBD acknowledges financial support from the NSF (CHE-1058805) and thanks Jorge Monteiro for assistance with photophysical data collection.

Notes and references

- 1 E. P. Horwitz and W. W. Schulz, *ACS Symp. Ser.*, 1999, **716**, 20.
- 2 (a) K. L. Nash, *Solv. Extr. Ion Exch.*, 1993, **11**, 729. (b) J. N. Mathur, M. S. Murali and K. L. Nash, *Solv. Extr. Ion Exch.*, 2001, **19**, 357. (c) K. L. Nash, in *Handbook on the Physics and Chemistry of Rare Earths*, K. A. Gschneider, L. Eyring, Jr., G. R. Choppin and G. H. Lander, (Eds.); Elsevier Science, Amsterdam, The Netherlands, 1994; Vol. 18, pp 197-238. (d) K. L.

Nash, C. Madic, J. N. Mathur and J. Lacquement, in *The Chemistry of the Actinide and Transactinide Elements*, L. R. Morss, N. M. Edelstein and J. Fuger (Eds.); Springer, Dordrecht, The Netherlands, 2006; Vol. 4, Ch 24, pp 2622-2798.

3 Z. Kolarik, *Chem. Rev.* 2008, **108**, 4208.

4 (a) C. Madic, M. Lecomte, P. Baron and B. Boullis, *C. R. Phys.* 2002, **3**, 797. (b) C. Madic and N. Ouvier, *Radiochim Acta* 2008, **96**, 183.

5 H. H. Dam, D. N. Reinhoudt and W. Verboom, *Chem. Soc. Rev.* 2007, **36**, 367 and references therein.

6 (a) S. A. Ansari, P. Pathak, P. K. Mohapatra and V. K. Manchanda *Chem. Rev.* 2012, **112**, 1751. (b) S. A. Ansari, P. N. Pathak, P. K. Mohapatra and V. K. Manchanda, *Sep. Purif. Rev.* 2011, **40**, 43 and references therein.

7 (a) F. W. Lewis, M. J. Hudson and L. M. Harwood, *Synlett*, 2011, 2609 and references therein. (b) M. J. Hudson, L. M. Harwood, D. M. Laventine and F. W. Lewis, *Inorg. Chem.* 2013, **52**, 3414.

8 (a) E. P. Horwitz, D. G. Kalina, H. Diamond, G. F. Vandergrift and W. W. Schulz, *Solv. Extr. Ion Exch.* 1985, **3**, 75. (b) W. W. Schulz, E. P. Horwitz, *Sep. Sci. Tech.* 1988, **23**, 1191. (c) E. P. Horwitz and W. W. Schulz, in *The TRUEX Process: A Vital Tool for the Disposal of U.S. Defense Waste*; Elsevier, London 1991, p 21.

9 C. Boehme and G. Wipff, *Inorg. Chem.* 2002, **41**, 727.

10 (a) E. P. Horwitz, D. G. Kalina, L. Kaplan, G. W. Mason and H. Diamond, *Sep. Sci. Tech.* 1982, **17**, 1261. (b) E. P. Horwitz and D. G. Kalina, *Solv. Extr. Ion Exch.* 1984, **2**, 179. (c) E. P.

- Horwitz, H. Diamond, K. A. Martin and R. Chiarizia, *Solv. Extr. Ion Exch.* 1987, **5**, 419. (d) E. P. Horwitz, H. Diamond and K. A. Martin, *Solv. Extr. Ion Exch.* 1987, **5**, 447. (e) E. P. Horwitz, K. A. Martin, H. Diamond and L. Kaplan, *Solv. Extr. Ion Exch.* 1986, **4**, 449.
- 11 (a) K. A. Martin, E. P. Horwitz and J. R. Ferraro, *Solv. Extr. Ion Exch.* 1986, **4**, 1149. (b) D. G. Kalina *Solv. Extr. Ion Exch.* 1984, **2**, 381.
- 12 (a) S. M. Bowen, E. N. Duesler and R. T. Paine, *Inorg. Chim. Acta* 1982, **61**, 155. (b) L. J. Caudle, E. N. Duesler and R. T. Paine, *R. T. Inorg. Chem.* 1985, **24**, 4441.
- 13 E. V. Sharova, O. I. Artyushin, Yu. V. Nelyubina, K. A. Lyssenko, M. P. Passechnik, and I. L. Odinet, *Russ. Chem. Bull. Intl. Ed.* 2008, **57**, 1890.
- 14 (a) M. W. Peters, E. J. Werner and M. J. Scott *Inorg. Chem.* 2002, **41**, 1707. (b) K. Matloka, A. K. Sah, M. W. Peters, P. Srinivasan, A. V. Gelis, M. Regalbuto and M. J. Scott, *Inorg. Chem.* 2007, **46**, 10549. (c) K. Matloka, A. K. Sah, P. Srinivasan and M. J. Scott, *C. R. Chimie* 2007, **10**, 1026.
- 15 M. Reinoso-García, D. Jańczewski, D. N. Reinhoudt, W. Verboom, E. Malinowska, M. Pietrzak, C. Hill, J. Bâca, B. Grüner, P. Selucky and C. Grüttner, *New J. Chem.* 2006, **30**, 1480.
- 16 V. Rudzevich, D. Schollmeyer, D. Braekers, J. F. Desreux, R. Diss, G. Wipff and V. Böhmer, *J. Org. Chem.* 2005, **70**, 6027.
- 17 (a) D. Jańczewski, D. N. Reinhoudt, W. Verboom, E. Malinowska, M. Pietrzak, C. Hill and C. Allignol, *New J. Chem.* 2007, **31**, 109. (b) H. H. Dam, D. N. Reinhoudt and W. Verboom, *New J. Chem.* 2007, **31**, 1620.

- 18 E. V. Sharova, O. I. Artyushin, A. N. Turanov, V. K. Karandashev, S. B. Meshkova, Z. M. Topilova and I. L. Odinets, *Cent. Eur. J. Chem.* 2012, **10**, 146.
- 19 (a) F. Arnaud-Neu, V. Böhmer, J.-F. Dozol, C. Grüttner, R. A. Jakobi, D. Kraft, O. Mauprivez, H. Rouquette, M.-J. Schwing-Weill, N. Simon and W. Vogt, *J. Chem. Soc. Perkin Trans.* 1996, **2**, 1175. (b) L. H. Delmau, N. Simon, M.-J. Schwing-Weill, F. Arnaud-Neu, J.-F. Dozol, S. Eymard, B. Tournois, V. Böhmer, G. Grüttner, C. Musigmann and A. Tunayar, *J. Chem. Soc., Chem. Commun.* 1998, 1627. (c) L. H. Delmau, N. Simon, M.-J. Schwing-Weill, F. Arnaud-Neu, J.-F. Dozol, S. Eymard, B. Tournois, C. Grüttner, C. Musigmann, A. Tunayar and V. Böhmer, *Sep. Sci. Tech.* 1999, **34**, 863. (d) A. Arduini, V. Böhmer, L. H. Delmau, J.-F., J.-F. Dozol, M. A. Garcia Carrera, B. Lambert, C. Musigmann, A. Pochini, A. Shivanyak and F. Ugozzoli, *Chem. Eur. J.* 2000, **6**, 2135. (e) B. Lambert, V. Jacques, A. Shivanyuk, S. E. Matthews, A. Tunayar, M. Baaden, G. Wipff, V. Böhmer and J. F. Desreux, *Inorg. Chem.* 2000, **39**, 2033. (f) F. Arnaud-Neu, S. Barbosa, V. Böhmer, F. Brisach, L. H. Delmau, J.-F. Dozol, O. Mogck, E. F. Paulus, M. Saadioui and A. Shivanyak, *Aust. J. Chem.* 2003, **56**, 1113. (g) V. A. Babain, M. Y. Alyapyshev, M. D. Karavan, V. Böhmer, L. Wang, E. A. Shokova, A. E. Motornaya, I. M. Vatsouro and V. V. Kovalev *Radiochim. Acta* 2005, **93**, 749. (h) A. Motornaya, I. Vatsouro, E. Shokova, V. Hubscher-Bruder, M. Alyapyshev, V. Babain, M. Karavan, F. Arnaud-Neu, V. Böhmer and V. Kovalev, *Tetrahedron* 2007, **63**, 4748. (i) C. Peters, D. Braekers, J. Kroupa, O. Kasyan, S. Miroshnichenko, V. Rudzevich and V. Böhmer, *Radiochim. Acta* 2008, **96**, 203. (j) F. Sansone, M. Galletta, E. Macerata, E. Trivellone, M. Giola, R. Ungaro, V. Böhmer, A. Casnati and R. Mariani *Radiochim. Acta* 2008, **96**, 235. (k) C. Dordea, F. Brisach, J. Haddaoui, F. Arnaud-Neu, M. Bolte, A. Casnati and V. Böhmer, *Supramol. Chem.* 2010, **22**,

347. (l) V. Vatsouro, A. Serebryannikova, L. Wang, V. Hubscher-Bruder, E. Shokova, M. Bolte, F. Arnaud-Neu, V. Böhmer and V. Kovalev, *Tetrahedron*, 2011, **67**, 8092.
- 20 (a) H. Boerrigter, V. Verboom and D. N. Reinhoudt, *J. Org. Chem.* 1997, **62**, 7148. (b) H. Boerrigter, W. Verboom and D. N. Reinhoudt, *Liebigs Ann. Recueil* 1997, 2247.
- 21 M. Ejaz and D. J. Carswell, *J. Inorg. Nucl. Chem.* 1975, **37**, 233. (b) M. Ejaz, *Sep. Sci.* 1975, **10**, 425. (c) M. Ejaz, *Microchim. Acta*, 1976, **65**, 643.
- 22 (a) V. K. Manchanda, J. P. Shukla and M. S. Subramanian, *J. Radioanal. Chem.* 1976, **29**, 69. (b) V. K. Manchanda, J. P. Shukla and M. S. Subramanian, *J. Inorg. Nucl. Chem.* 1974, **36**, 2595.
- 23 (a) D. J. McCabe, A. A. Russell, S. Karthikeyan, R. T. Paine, R. R. Ryan and B. Smith, *Inorg. Chem.* 1987, **26**, 1230. (b) G. S. Conary, A. A. Russell, R. T. Paine, J. H. Hall and R. R. Ryan, *Inorg. Chem.* 1988, **27**, 3242. (c) A. A. Russell, R. L. Meline, E. N. Duesler and R. T. Paine, *Inorg. Chim. Acta* 1995, **231**, 1.
- 24 (a) B. M. Rapko, E. N. Duesler, P. H. Smith, R. T. Paine and R. R. Ryan, *Inorg. Chem.* 1993, **32**, 2164. (b) U. Engelhardt, B. M. Rapko, E. N. Duesler, D. Frutos and R. T. Paine, *Polyhedron* 1995, **14**, 2361. (c) E. M. Bond, X. Gan, J. R. FitzPatrick and R. T. Paine, *J. Alloys Compds.* 1998, **271-273**, 172. (d) E. M. Bond, E. N. Duesler, R. T. Paine, M. P. Neu, J. H. Matonic and B. L. Scott, *Inorg. Chem.* 2000, **39**, 4152. (e) E. M. Bond, E. N. Duesler, R. T. Paine and H. Nöth, *Polyhedron*, 2000, **19**, 2135. (f) X.-M. Gan, S. Parveen, W. L. Smith, E. N. Duesler and R. T. Paine, *Inorg. Chem.* 2000, **39**, 4591. (g) J. H. Matonic, M. P. Neu and A. E. Enriquez, *J. Chem. Soc., Dalton Trans.* 2002, 2328. (h) X.-M. Gan, X.-M., E. N. Duesler and R. T. Paine, *Inorg. Chem.* 2001, **40**, 4420. (i) J. H. Matonic, A. E. Enriquez, B. L. Scott, R. T.

Paine and M. P. Neu, *Nucl. Sci. Tech.* 2002, **3**, 100. (j) R. T. Paine, E. M. Bond, S. Parveen, N. Donhart, E. N. Duesler, K. A. Smith and H. Nöth, *Inorg. Chem.* 2002, **41**, 444. (k) X.-M. Gan, R. T. Paine, E. N. Duesler and H. Nöth, *Dalton Trans.* 2003, 153. (l) X.-M. Gan, B. M. Rapko, E. N. Duesler, I. Binyamin, R. T. Paine and B. P. Hay, *Polyhedron*, 2005, **24**, 469. (m) S. Pailloux, C. E. Shirima, A. D. Ray, E. N. Duesler, R. T. Paine, J. R. Klaehn, M. E. McIlwain and B. P. Hay, *Inorg. Chem.* 2009, **48**, 3104. (n) S. Pailloux, C. E. Shirima, A. D. Ray, E. N. Duesler, K.A. Smith, R. T. Paine, J. R. Klaehn, M. E. McIlwain and B. P. Hay, *Dalton Trans.* 2009, 7486.

25 S. L. Blaha, D. J. McCabe, R. T. Paine and K. W. Thomas, *Radiochim. Acta* 1989, **46**, 123.

26 (a) E. M. Bond, U. Engelhardt, T. P. Deere, B. M. Rapko and R. T. Paine, *Solv. Extr. Ion Exch.* 1997, **15**, 381. (b) E. M. Bond, U. Engelhardt, T. P. Deere, B. M. Rapko and R. T. Paine, *Solv. Extr. Ion Exch.* 1998, **16**, 967. (c) K. L. Nash, C. Lavallette, M. Borkowski, R. T. Paine and X.-M. Gan, *Inorg. Chem.* 2002, **41**, 5849. (d) J. Sulakova, R. T. Paine, M. Chakravarty and K. L. Nash, *Sep. Sci. Tech.* 2012, **47**, 2015.

27 (a) D. Rosario-Amorin, S. Ouizem, D. A. Dickie, Y. Wen, R. T. Paine, A. de Bettencourt-Dias, B. P. Hay and L. H. Delmau, *Inorg. Chem.* 2013, **52**, 3063. (b) D. Rosario-Amorin, D. A. Dickie, Y. Wen and R. T. Paine, *Phosphorus, Sulfur, Silicon Relat. Elem.* 2013, **188**, 100.

28 M. Woods and A. D. Sherry, *Inorg. Chem.* 2003, **42**, 4401.

29 T. Gunnlaugsson, D. F. Brougham, A.-M. Fanning, M. Nieuwenhuyzen, J. E. O'Brien and R. Viguier, *Org. Lett.* 2004, **6**, 4805.

30 (a) L. J. Caudle, E. N. Duesler and R. T. Paine *Inorg. Chim. Acta* 1985, **110**, 91. (b) L. J. Caudle, PhD Thesis, University of New Mexico, 1983.

- 31 M. Yu. Antipin, Yu. T. Struchkov, E. I. Matrosov, M. I. Kabachnik, *J. Struct. Chem.* 1985, **26**, 441.
- 32 N. Narayanaswamy, D. Maity and T. Govindaraju, *Supramolecular Chem.* 2011, **23**, 703.
- 33 P. Roquette, C. König, O. Hübner, A. Wagner, E. Kaifer, M. Enders and H.-J. Himmel, *Eur. J. Inorg. Chem.* 2010, 4770.
- 34 B. P. Hay, A. A. Oliferenko, J. Uddin, C. Zhang and T. K. Firman, *J. Am. Chem. Soc.* 2005, **127**, 17043.
- 35 The structure adopted by free **18** in the solid state is not a minimum on the MM3 potential energy surface. The structure obtained when starting from the crystal structure coordinates lies 9.8 kcal/mole higher in energy than the energy of the computed gas phase global minimum structure. The observed form in the crystal structure is stabilized by the intermolecular hydrogen bonding described above.
- 36 P. A. Brayshaw, J.-C. G. Bünzli, P. Froidevaux, J. M. Harrowfield, Y. Kim and A. N. Sobolev, *Inorg. Chem.* 1995, **34**, 2068.
- 37 (a) F. A. Cotton, *Chemical Applications of Group Theory*, 2nd ed, Wiley-Interscience: New York, 1963. (b) P. A. Tanner, Lanthanide Luminescence in Solid, in *Lanthanide Luminescence: Photophysical, Analytical and Biological Aspects*; P. Hänninen and H. Härrma, H. (Eds.); Springer Series in Fluorescence, 2011; Vol 7, pp. 183-234.
- 38 A. de Bettencourt-Dias, P. S. Barber and S. Bauer, *J. Am. Chem. Soc.* 2012, **134**, 6987.
- 39 (a) J. Andres and A.-S. Chauvin, *Inorg. Chem.* 2011, **50**, 10082. (b) E. Deiters, B. Song, A.-S. Chauvin, C. D. B. Vandevyver, F. Gumy and J.-C. G. Bünzli, *Chem. Eur. J.* 2009, **15**, 885.

- 40 A. de Bettencourt-Dias, *Curr. Org. Chem.* 2007, **11**, 1460.
- 41 W. D. Horrocks, Jr. and D. R. Sudnick, *Acc.Chem.Res.* 1981, **14**, 384. W. D. Horrocks, Jr. and D. R. Sudnick, *J. Am. Chem. Soc.* 1979, **101**, 334.
- 42 For ease of viewing, additional schematic representations of the Ln(III)-ligand binding interactions are shown in the ESI (S.90).
- 43 R. D. Shannon and T. C. Prewitt, *Acta Crystallogr.*, Sect. B 1969, **B25**, 925.
- 44 The C- and H-atom numbering systems employed for the NMR chemical shift assignments are given for all of the compounds in the Electronic Supplementary Information (ESI).
- 45 *APEX 2*; Bruker AXS, Inc.: Madison, WI, 2007. (b) SAINT + 7.01, 2003 Bruker AXS, Inc., Madison, WI 53719. (c) SADABS 2.10, 2003, G. M. Sheldrick, University of Gottingen: Gottingen, Germany.
- 46 SHELXL-97, 2008, Bruker AXS, Inc., Madison, WI 53719.
- 47 (a) P. van der Sluis and A. L. Spek, *Acta Crystallogr.* 1990, **A46**, 194. (b) A. L. Spek, *Acta Crystallogr.* 1990, **A46**, C34.
- 48 (a) N. L. Allinger, Y.-H. Yuh and J.-H. Lii, *J. Am. Chem. Soc.* 1989, **111**, 8551. (b) J.-H. Lii and N. L. Allinger, *J. Am. Chem. Soc.* 1989, **111**, 8566. (c) J.-H. Lii and N. L. Allinger, *J. Am. Chem. Soc.* 1989, **111**, 8576.
- 49 B. P. Hay, *Coord. Chem. Rev.* 1993, **126**, 177.
- 50 PCModel, version 9.3, Serena Software, Bloomington, Indiana.

Table 1. Selected Bond Lengths for **6**·2H₂O, **7**, **12**, **18**·MeOH (Å)

Bond Type	6 ·2H ₂ O		7		12		18 ·MeOH	
P-O	P1-O3	1.4845(14)	P1-O3	1.4847(14)	P1-O1	1.4927(13)	P1-O1	1.4916(18)
			P2-O4	1.4945(14)				
N-O	N1-O1	1.325(2)	N1-O1	1.308(2)				
C-O	C7-O2	1.228(2)	C7-O2	1.227(2)	C7-O2	1.223(42)	C5-O2	1.225(3)

Table 2. Lifetimes τ [μs] of [Eu(**6**)(NO₃)₃] and [Eu(**7**)(NO₃)₃] in the solid state and in methanol solution at 25°C and number of methanol molecules n_{MeOH} coordinated to the europium in methanol solution.

		[Eu(6)(NO ₃) ₃]	[Eu(7)(NO ₃) ₃]
τ [μs]	Solid	562 \pm 2	875 \pm 3
	MeOH	380 \pm 77	782 \pm 7
	<i>d</i> ⁶ -MeOD	1326 \pm 211	1708 \pm 11
n_{MeOH}		4	1.5

Table 3. Selected Bond Lengths for Coordination Complexes (Å)

Bond	{[Yb(6)(NO ₃) ₃](Me		{[Er(6) ₂ (H ₂ O) ₂]		{[Eu(7)(NO ₃) ₂ (EtOAc) _{0.5}		[Dy ₃ (7) ₄ (NO ₃) ₄ (H ₂ O) ₂]({[La(13)(NO ₃) ₃ (MeOH)]	
Type	OH)} _n		(NO ₃) ₃ ·(H ₂ O) ₄ } _n		(H ₂ O) _{0.5}] (NO ₃) ₂ ·MeOH		NO ₃) ₅ ·(MeOH) ₅ ·(H ₂ O) ₂		·(MeOH)} _n	
M-O(P)	Yb1-O3	2.271(3)	Er1-O3	2.272(3)	Eu1-O3	2.381(2)	Dy1-O7	2.353(7)	La1-O2	2.467(2)
					Eu1-O4	2.350(2)	Dy1-O4	2.332(7)	La1-O3a	2.411(2)
							Dy2-O3	2.311(7)		
							Dy2-O8	2.378(7)		
M-O(N) _{pyr}	Yb1-O1a	2.241(3)	Er1-O1	2.324(3)	Eu1-O1	2.322(2)	Dy1-O1	2.304(7)		
							Dy2-O5	2.346(7)		
M-O(C)	Yb1-O2	2.268(3)	Er1-O2b	2.430(3)	Eu1-O2	2.444(3)	Dy1-O6	2.411(7)	La1-O1	2.551(2)
							Dy2-O2	2.446(7)		
M-O _{nitrate}	2.43 ± 0.06				2.53 ± 0.05		2.51 ± 0.02		2.65 ± 0.03	
Avg	2.380(3)-2.545(3)				2.471(3)-2.613(3)		2.487(7)-2.535(6)		2.606(2)-2.698(2)	
Range										
M-O _(solv)			Er1-O9	2.365(3)	Eu1-O14	2.497(7)	Dy1-O23	2.365(7)	La1-O13	2.624(2)
					Eu1-O16	2.349(8)				
P-O	P1-O3	1.505(3)	P1-O3	1.503(3)	P1-O3	1.506(3)	P2-O4	1.493(7)	P1-O2	1.499(2)
							P3-O7	1.509(8)	P2-O3	1.502(2)
							P1-O3	1.499(8)		

						P4-O8	1.498(8)		
N-O	N1-O1	1.337(5)	N1-O1	1.340(5)	N1-O1	1.330(4)	N1-O1	1.324(11)	
							N3-O5	1.331(11)	
C-O	C7-O2	1.241(5)	C7-O2	1.238(6)	C7-O2	1.246(4)	C40-O6	1.216(13)	C7-O1 1.245 (4)
							C7-O2	1.255(13)	

Table 4. Crystallographic Data for **6·2H₂O**, **7**, **12**, **18·MeOH**

	6·2H₂O	7	12	18·MeOH
empirical formula	C ₂₀ H ₂₃ N ₂ O ₅ P	C ₃₃ H ₃₀ N ₂ O ₄ P ₂	C ₂₁ H ₂₀ ClN ₂ O ₂ P	C ₃₆ H ₃₇ N ₃ O ₅ P ₂
crystal size (mm)	0.22 x 0.22 x 0.26	0.15 x 0.24 x 0.35	0.17 x 0.21 x 0.42	0.10 x 0.19 x 0.24
formula weight	402.38	580.55	398.82	653.63
crystal system	triclinic	monoclinic	triclinic	orthorhombic
space group	<i>P-1</i>	<i>P2(1)/n</i>	<i>P-1</i>	<i>Pnma</i>
unit cell dimen.				
<i>a</i> (Å)	9.5148(4)	14.8196(13)	10.0038(4)	18.635(2)
<i>b</i> (Å)	10.5452(4)	12.6867(10)	10.2770(4)	31.142(3)
<i>c</i> (Å)	10.9891(4)	116.4438(14)	11.3976(4)	5.6670(6)
<i>α</i> (°)	67.994(2)	106.043(3)	111.639(2)	90
<i>β</i> (°)	85.172(2)	90	114.435(2)	90
<i>γ</i> (°)	81.411(2)	109.425(5)	95.410(2)	90
<i>V</i> (Å ³)	1010.32(7)	90	948.52(6)	3288.7(6)
<i>Z</i>	2	4	2	4
T, (K)	173(2)	173(2)	173(2)	100(2)
D _{calcd} (g cm ⁻³)	1.323	1.323	1.396	1.320
<i>μ</i> (mm ⁻¹)	0.169	0.190	0.305	0.180

min/max transmission	0.9576/0.9635	0.9362/0.9716	0.8818/0.9494	0.9581/0.9829
reflection collected	15916	27090	8778	24824
independent reflections [R _{int}]	3966[0.0391]	6400[0.0556]	3724[0.0247]	3186[0.1035]
final R indices [I > 2σ (I)]	0.0395(0.1029)	0.0423(0.0994)	0.0382(0.0871)	0.0476(0.0976)
R1 (wR2)				
final R indices (all data) R1(wR2)	0.0589(0.1149)	0.0681(0.1135)	0.0514(0.0937)	0.0870(0.1127)

Table 5. Crystallographic Data for Coordination Complexes

	{[Yb(6)(NO ₃) ₃]}·(MeOH) _n	{[Er(6) ₂ (H ₂ O) ₂](NO ₃) ₃ ·(H ₂ O) ₄] _n	{[Eu(7)(NO ₃) ₂ (EtOAc) _{0.5} (H ₂ O) _{0.5}](NO ₃) ₂ ·(MeOH)}	[Dy ₃ (7) ₄ (NO ₃) ₄ (H ₂ O) ₂](NO ₃) ₅ ·(MeOH) ₅ ·(H ₂ O) ₂	{[La(13)(NO ₃) ₃ (MeOH)]·(MeOH) _n }
empirical formula	C ₂₁ H ₂₃ N ₅ O ₁₃ PYb	C ₄₀ H ₅₀ ErN ₇ O ₂₁ P ₂	C ₇₁ H ₇₄ Eu ₂ N ₁₀ O ₃₀ P ₄	C ₁₃₇ H ₁₄₈ Dy ₃ N ₁₇ O ₅₂ P ₈	C ₃₅ H ₃₈ LaN ₅ O ₁₄ P ₂
Crystal size (mm)	0.12 x 0.22 x 0.23	0.17 x 0.28 x 0.28	0.29 x 0.44 x 0.51	0.16 x 0.19 x 0.32	0.11 x 0.23 x 0.25
formula weight	757.45	1194.07	1975.22	3599.98	953.55
crystal system	monoclinic	monoclinic	monoclinic	orthorhombic	orthorhombic
space group	<i>P2₁/c</i>	<i>P2₁/c</i>	<i>P2₁/c</i>	<i>C222₁</i>	<i>Pca2₁</i>
unit cell dimen.					
<i>a</i> (Å)	16.7262(19)	13.1332(9)	11.0923(9)	16.1711(5)	24.7829(16)
<i>b</i> (Å)	11.4988(12)	11.4606(8)	25.3538(18)	36.6811(13)	8.7977(6)
<i>c</i> (Å)	14.6506(17)	16.4028(11)	18.0674(14)	28.7076(10)	18.1338(12)
<i>α</i> (°)	90	90	90	90	90
<i>β</i> (°)	109.599(6)	92.252(3)	104.373(4)	90	90
<i>γ</i> (°)	90	90	90	90	90
<i>V</i> (Å ³)	2654.5(5)	2467.0(3)	4922.1(7)	17028.6(10)	3953.8(5)
<i>Z</i>	4	2	2	4	4
T, K	173(2)	173(2)	173(2)	100(2)	100(2)
<i>D</i> _{calcd} (gcm ⁻³)	1.895	1.607	1.333	1.404	1.602

μ (mm ⁻¹)	3.660	1.851	1.401	1.460	1.234
min/max transmission	0.4865/0.6762	0.6243/0.7499	0.5350/0.6880	0.6550/0.7970	0.7478/0.8762
reflection collected	23042		56754	83047	47044
independent reflections	5854[0.0509]	5076[0.0]	11283[0.0249]	17393[0.1087]	8387[0.0445]
[R _{int}]					
final R indices [I > 2 σ (I)]	0.0329(0.0667)	0.0342(0.0970)	0.0418(0.0990)	0.0524(0.1209)	0.0233(0.0476)
R1 (wR2)					
final R indices (all data)	0.0527(0.0730)	0.0440(0.1258)	0.0452(0.1006)	0.0809(0.1349)	0.0288(0.0495)
R1(wR2)					

Synopsis (Table of Contents Graphic)**Synthesis and f-element ligation properties of ^NCMPO-decorated pyridine N-oxide platforms.**

Sabrina Ouizem, Daniel Rosario-Amorin, Diane A. Dickie, Robert T. Paine, A. de Bettencourt-Dias, Benjamin P. Hay, Julien Podair and Lætitia H. Delmau

Syntheses for hybrid N-attached CMPO decorated pyridine N-oxide ligands, computational, spectroscopic and structural characterization of their coordination interactions with lanthanide ions and survey solvent extraction analyses are described.

